



Article

Global Proteomics for Identifying the Alteration Pathway of Niemann–Pick Disease Type C Using Hepatic Cell Models

Keitaro Miyoshi ^{1,†}, Eiji Hishinuma ^{2,3,†}, Naomi Matsukawa ³, Yoshitaka Shirasago ⁴, Masahiro Watanabe ⁵, Toshihiro Sato ⁶ , Yu Sato ⁶ , Masaki Kumondai ⁶ , Masafumi Kikuchi ^{1,5,6}, Seizo Koshiba ^{2,3}, Masayoshi Fukasawa ⁴ , Masamitsu Maekawa ^{1,2,5,6,*} and Nariyasu Mano ^{1,5,6}

¹ Faculty of Pharmaceutical Sciences, Tohoku University, 1-1 Seiryō-machi, Aoba-Ku, Sendai 980-8574, Japan

² Advanced Research Center for Innovations in Next-Generation Medicine, Tohoku University, 2-1 Seiryō-machi, Aoba-Ku, Sendai 980-8573, Japan; ehishi@ingem.oas.tohoku.ac.jp (E.H.)

³ Tohoku Medical Megabank Organization, Tohoku University, 2-1 Seiryō-machi, Aoba-Ku, Sendai 980-8573, Japan

⁴ Department of Biochemistry and Cell Biology, National Institute of Infectious Diseases, 1-23-1, Toyama, Shinjuku-ku, Tokyo 162-8640, Japan

⁵ Graduate School of Pharmaceutical Sciences, Tohoku University, 1-1 Seiryō-machi, Aoba-Ku, Sendai 980-8574, Japan

⁶ Department of Pharmaceutical Sciences, Tohoku University Hospital, 1-1 Seiryō-machi, Aoba-Ku, Sendai 980-8574, Japan

* Correspondence: m-maekawa@tohoku.ac.jp; Tel.: +81-22-717-7541

† The authors contributed to this work equally.

Abstract: Niemann–Pick disease type C (NPC) is an autosomal recessive disorder with progressive neurodegeneration. Although the causative genes were previously identified, NPC has unclear pathophysiological aspects, and patients with NPC present various symptoms and onset ages. However, various novel biomarkers and metabolic alterations have been investigated; at present, few comprehensive proteomic alterations have been reported in relation to NPC. In this study, we aimed to elucidate proteomic alterations in NPC and perform a global proteomics analysis for NPC model cells. First, we developed two NPC cell models by knocking out *NPC1* using CRISPR/Cas9 (KO1 and KO2). Second, we performed a label-free (LF) global proteomics analysis. Using the LF approach, more than 300 proteins, defined as differentially expressed proteins (DEPs), changed in the KO1 and/or KO2 cells, while the two models shared 35 DEPs. As a bioinformatics analysis, the construction of a protein–protein interaction (PPI) network and an enrichment analysis showed that common characteristic pathways such as ferroptosis and mitophagy were identified in the two model cells. There are few reports of the involvement of NPC in ferroptosis, and this study presents ferroptosis as an altered pathway in NPC. On the other hand, many other pathways and DEPs were previously suggested to be associated with NPC, supporting the link between the proteome analyzed here and NPC. Therapeutic research based on these results is expected in the future.

Keywords: Niemann–Pick disease type C; global proteomics; liquid chromatography–electrospray ionization tandem mass spectrometry; model cell; knock out; enrichment pathway analysis



Citation: Miyoshi, K.; Hishinuma, E.; Matsukawa, N.; Shirasago, Y.; Watanabe, M.; Sato, T.; Sato, Y.; Kumondai, M.; Kikuchi, M.; Koshiba, S.; et al. Global Proteomics for Identifying the Alteration Pathway of Niemann–Pick Disease Type C Using Hepatic Cell Models. *Int. J. Mol. Sci.* **2023**, *24*, 15642. <https://doi.org/10.3390/ijms242115642>

Academic Editor: Ritva Tikkanen

Received: 27 September 2023

Revised: 24 October 2023

Accepted: 25 October 2023

Published: 27 October 2023



Copyright: © 2023 by the authors. Licensee MDPI, Basel, Switzerland. This article is an open access article distributed under the terms and conditions of the Creative Commons Attribution (CC BY) license (<https://creativecommons.org/licenses/by/4.0/>).

1. Introduction

Niemann–Pick disease type C (NPC) is a progressive and life-limiting autosomal recessive disorder characterized by progressive neurodegeneration [1–3]. Due to the development of laboratory medicines for NPC [2,4–9], the number of NPC patients is increasing, and the current estimated prevalence is approximately 1/100,000 [10]. NPC is caused by mutations in *NPC1* or *NPC2*. *NPC1* codes for the NPC1 cholesterol transport membrane protein in lysosomes, whereas *NPC2* codes for the NPC2 intracellular cholesterol-binding soluble protein in lysosomes [11]. *NPC1* and *NPC2* coordinate in the transport of cholesterol, and *NPC1* or *NPC2* mutations can cause cholesterol traffic dysfunction [12,13]. Although

NPC is not related to enzyme deficiency, it is considered a lysosomal storage disease (LSD). In addition, various sphingolipids, including sphingomyelin [14,15] and glycosphingolipids, [16,17] accumulate in NPC. Glycosphingolipid metabolism is a therapeutic target pathway in NPC, and miglustat, which inhibits glucosylceramide synthase, is currently the only approved drug [18].

The pathophysiology of NPC involves patients presenting a variety of symptoms. The onset age of NPC symptoms varies from the neonatal to adulthood, and the clinical symptoms also differ widely [1,2,10]. Hepatosplenomegaly and cholestasis are typical symptoms, and many patients develop various neurodegenerative disorders depending on their age [1]. Disease prognosis is generally improved when treatment begins earlier [18]; therefore, earlier diagnosis is desired, and a number of clinical biomarkers have been developed for the early discovery of this condition [4–7]. Since 2010, oxysterols [19,20], lysosphingomyelin [14,21], *N*-palmitoyl-*O*-phosphocholine-serine [22–25] (previously called Lyso-SM-509), and abnormal bile acids containing conjugates [8,9,26–33] have been reported as biomarkers of NPC. However, the detailed mechanisms underlying the progression of this disease remain unknown [10].

Proteomics is an omics analytical technique used to elucidate the molecular and pathophysiological alterations in expressed cellular proteins [34–42]. Although the genome is static, the proteome is dynamic [43–45] and has a longer turnover time than the metabolome [46,47]. Liquid chromatography–tandem mass spectrometry (LC/MS/MS) is commonly used for proteomic analyses [41,48–50], particularly in the form of nanoLC/MS/MS [41,50,51]. In searching for the alteration pathways of various diseases, an untargeted proteomics approach called global proteomics has been widely used [41,52].

In this study, to reveal the pathophysiology in the proteomic aspects of NPC and discover novel therapeutic targets, we aimed to elucidate the altered pathway in NPC model cells using the global proteomics approach.

2. Results and Discussion

2.1. NPC Model Cell Development

Gene editing was performed on *NPC1* by knocking out *NPC1* using the CRISPR/Cas9 method [53–55]. We attempted to target two different gene sites simultaneously. One approach focused on sites A and C (for KO1 cells), and the other focused on sites B and D (for KO2 cells). Sites A and B were located in the signal sequences, Site C was located on exon 8, which is included in the first extracellular loop, and Site D was located on exon 22, which is in ninth transmembrane region. As a result of the mutation, NPC1 proteins were not detected via immunoblotting in either KO1 or KO2 (Figure S1). Filipin staining, which is the gold-standard method for NPC diagnosis of patients [56], was then performed, and cholesterol accumulation was observed in both the KO1 and KO2 cells (Figure S2). In addition, enzymatic free-cholesterol quantitation showed a significant difference between the KO and WT cells (Figure 1).

NPC is caused by a lack of function of NPC1 or NPC2 [1]. A representative NPC cell phenotype is the accumulation of lysosomal free cholesterol [12,13,57]. In the present study, cell DNA editing engineering was successful (Figure S3a), and two types of NPC1 model cells were developed (KO1 and KO2). In the KO1 cells, mutations of exon 1 and exon 8 were targeted. Exon 8 contains the second transmembrane region and the 1st extracellular loop (Figure S3a,b). Therefore, gene editing provided an NPC 1 protein that was undetectable via immunoblotting with the NPC1 antibody. In the KO2 cells, mutations in the signal sequences on exon 1 and the ninth transmembrane region on exon 22 were identified (Figure S3a,c). Similar to the KO1 cells, we succeeded in developing NPC1 mutant cells. Both filipin staining and enzymatic quantification provided the representative NPC phenotypes.

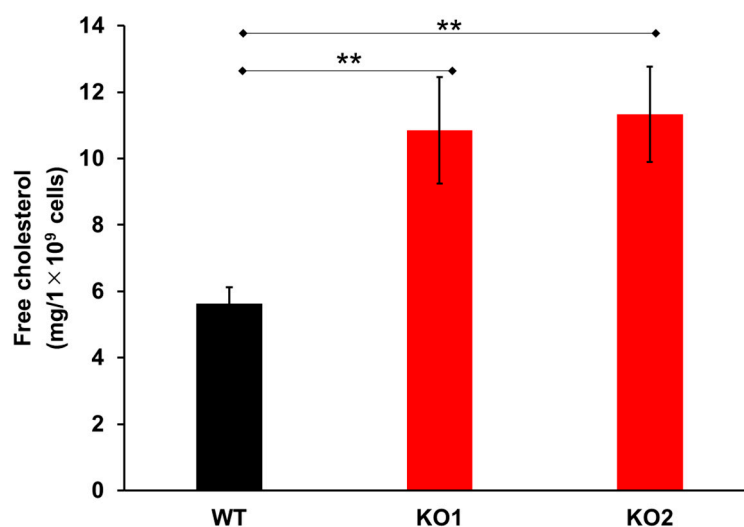


Figure 1. Accumulated cholesterol quantitation in wild-type cells and two types of NPC1 knockout cells. Data represent the means \pm SDs, $n = 9$, $** p < 0.01$ (two-tailed Welch's *t*-test). WT—Hep G2 cells; KO1—Sites A and C mutant NPC1 model cells; KO2—Sites B and D mutant NPC1 model cells.

2.2. Label-Free Global Proteomics

We then performed a global proteomics analysis known as the label-free (LF) method. The global method is a nontargeted approach that does not define specific molecules as analytes and covers a wide range of molecule sizes.

First, we summarized the protein numbers identified from the LF global proteomics analysis (Figure 2, Tables S1 and S2). The regions that were not overlaid with any other regions contained a few proteins. Each cell line was analyzed in five biological replicates, and proteins identified in four or more replicates were used for a subsequent pathway analysis. As a result, a total of 3331 proteins were identified in all cell types, 3390 proteins were identified in the WT and KO1 cells, 3434 proteins were identified in the WT and KO2 cells (Figure 2).

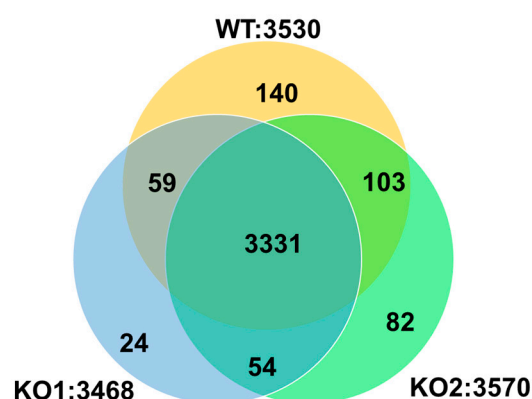


Figure 2. Venn diagram showing protein numbers identified from the results of the label-free global proteomics analysis. WT—Hep G2 cells; KO1—Sites A and C mutant NPC1 model cells; KO2—Sites B and D mutant NPC1 model cells.

Second, we investigated the characteristics of each sample using a multivariate analysis. A principal component analysis (PCA) was first performed using 3331 proteins whereby three samples (WT, KO1, and KO2) were plotted closely for each group. In addition, the KO1 and KO2 cells were shown in different areas (Figure 3a). This indicates that the characteristics of the NPC1 model cells are different from those of WT cells, and the proteins expressed in the KO1 and KO2 cells also differ from each other. NPC1 showed clinically diverse phenotypes [1,2,10]. In NPC patients, the gene mutations of *NPC1* vary

by race [58–61] and various gene mutations are known, with novel mutations currently being reported [62]. However, a detailed correlation between gene mutations and clinical phenotypes remains unknown [10]. In this study, the KO1 cells, which have two mutation sites on the signal sequence on exon 1 and the first extracellular loop on exon 8, and the KO2 cells, which have two mutation sites on the signal sequence on exon 1 and the ninth transmembrane region on exon 22, showed different results in the PCA. We also utilized a loading plot in order to infer which proteins are responsible for the difference in each type of cell (Figure 3b). In the loading plot, the cumulative contribution ratio of the first and second principal components (PC1 and PC2) was 93.3%, which is a large amount of information. Keratin, type II cytoskeletal 8 (KRT8), Keratin, type I cytoskeletal 18 (KRT18), 60 kDa heat shock protein, mitochondrial (HSPD1), Actin, cytoplasmic 1 (ACTB), and Vimentin (VIM) represent some of the largest absolute values of the major components of both PC1 and PC2. These proteins could be responsible for the differences among cell types.

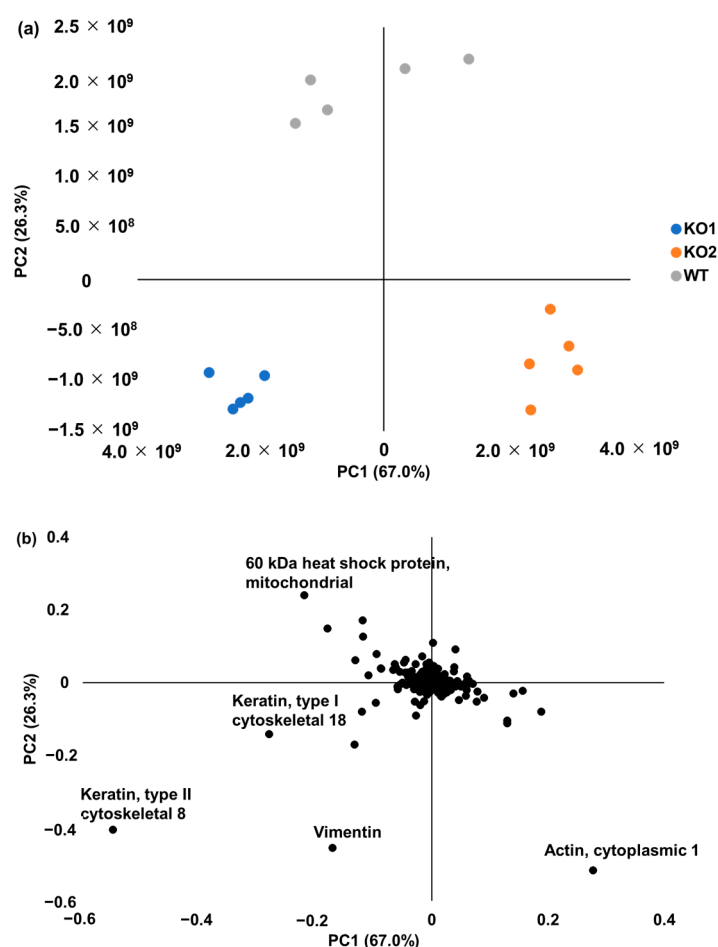


Figure 3. The principal component analysis of the LF method. (a) A PCA plot using 3331 proteins identified in the KO1, KO2, and WT cells. (b) A loading plot using 3331 proteins identified in the KO1, KO2, and WT cells. WT—Hep G2 cells; KO1—Sites A and C mutant NPC1 model cells; KO2—Sites B and D mutant NPC1 model cells.

Finally, we created a volcano plot which shows the degree of change and statistical significance simultaneously on the graph [63–65] (Figure 4). The selection criteria for differentially expressed proteins (DEPs) were set at a two-fold change and statistical significance ($p < 0.05$) between the NPC1 model and WT cells. The identified DEPs are summarized in Figure S4, Table 1, and Table S3. In Figure S4, the total numbers of DEPs which were both up- and downregulated in the NPC1 model cells are shown. The overlap of the two

model cells is presented in Table 1. Twenty-five proteins were upregulated in both the KO1 and KO2 cells, and 10 proteins were downregulated. Two proteins increased in KO1 cells but decreased in KO2 cells, and four proteins decreased in both KO1 and KO2 cells. Other proteins were either upregulated or downregulated in KO1 or KO2 cells only. The overlapping protein numbers were low among the total DEPs. The common DEPs in the KO1 and KO2 cells were not the main DEPs observed. In addition, there were proteins that were upregulated in the KO1 cells but were downregulated in the KO2 cells and vice versa. As mentioned above, the NPC phenotype is diverse, and patients with NPC have varied symptoms [1,2]. Therefore, the proteomic results for the KO1 and KO2 cells indicate that the difference in mutation sites between the KO1 and KO2 cells affects the proteomic expression pattern.

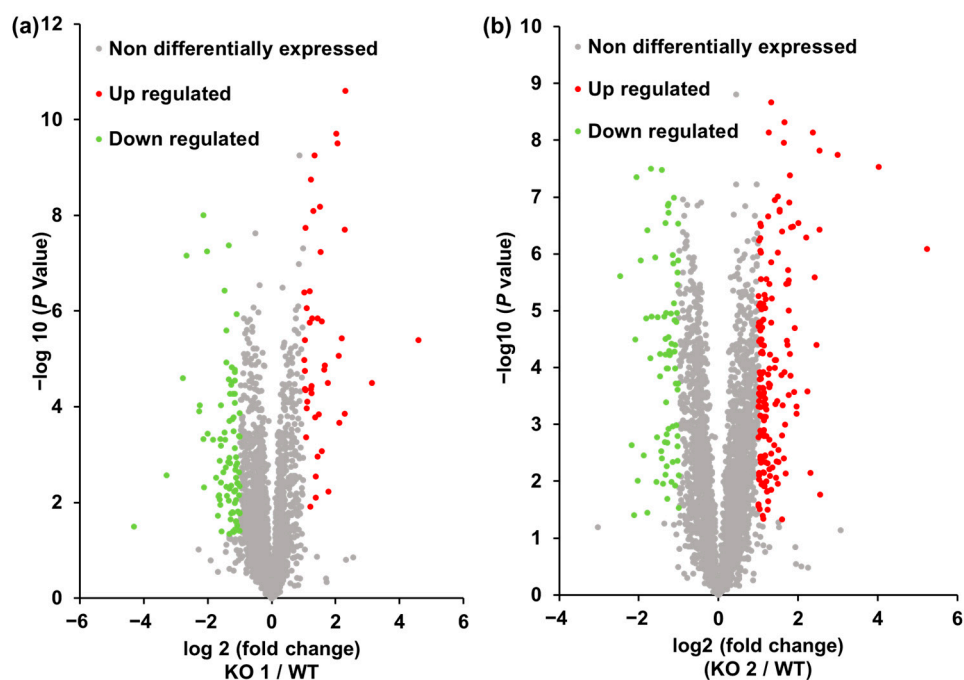


Figure 4. Volcano plots from the results of the label-free global proteomics analysis. (a) KO1 versus WT using 3390 proteins identified in KO1 and WT cells. (b) KO2 versus WT using 3434 proteins identified in KO2 and WT cells. Red-colored plots—greater than 2-fold upregulated and $p < 0.05$ (adjusted using the Benjamini–Hochberg correction) proteins in NPC1 model cells; green-colored plots—greater than 0.5-fold downregulated and $p < 0.05$ (adjusted using the Benjamini–Hochberg correction) proteins in NPC1 model cells; grey-colored plots—non-differentially changed proteins. WT—Hep G2 cells; KO1—Sites A and C mutant NPC1 model cells; KO2—Sites B and D mutant NPC1 model cells.

Table 1. Summary of protein numbers of DEPs in the label-free global proteomics analysis.

	Upregulated DEPs (Numbers)		Downregulated DEPs (Numbers)		Total (Numbers)
Identified in KO1 (numbers)	18		77		95
	25	(a) 2	(b) 4	10	35 (41)
Identified in KO2 (numbers)	145		63		208
Total	188	6	150	338 (344)	

(a) are identified as upregulated DEPs in KO1 cells and downregulated DEPs in KO2 cells, (b) are identified as downregulated DEPs in KO1 cells and upregulated DEPs in KO2 cells. WT—hep G2 cells; KO1—Sites A and C mutant NPC1 model cells; KO2—Sites B and D mutant NPC1 model cells.

2.3. Bioinformatics Analysis

We evaluated the interaction of the DEPs using the Search Tool for the Retrieval of Interacting Genes/Proteins (STRING). The DEPs of the KO1 cells provided us with a protein–protein interaction (PPI) network consisting of 136 nodes and 154 edges. The expected number of edges from the number of nodes was 96, which is a much lower value than the actual edges, and the PPI enrichment p value was 3.36×10^{-8} (Figure S5a). The DEPs of the KO2 cells provided us with a PPI network consisting of 249 nodes and 855 edges. The expected number of edges from the number of nodes was 452, which is a much lower value than the actual edges, and the PPI enrichment p value was $<1.0 \times 10^{-16}$ (Figure S5c). The nodes of the upregulated proteins in the DEPs were displayed in red, and downregulated proteins were displayed in green. These results show the overall picture of up/downregulation and protein–protein interactions in the DEPs and suggest that the DEPs have strong interactions in the KO1 and KO2 cells. In addition, an analysis excluding text mining from the interaction sources showed 71 edges in the KO1 cells and 518 edges in the KO2 cells, with percentages of 46.1% and 60.6%, respectively. It was confirmed that there were enough reliable edges other than text mining, such as curated databases, experiments, and co-expression.

In addition, we displayed the proteins coded via ferroptosis in blue and those coded via ribosome biogenesis in eukaryotes in yellow. These pathways were identified as particularly significant in the enrichment analysis (ferroptosis was the highest in both KO1 and KO2 cells, and ribosome biogenesis in eukaryotes was the second highest in the KO2 cells, Figure 5). In particular, ferroptosis was identified for both KO1 and KO2 cells. Marked proteins are linked by many edges and are in regions with many edges in the figure, suggesting strong interactions of the DEPs in each cell at these pathways (Figure S5b,d).

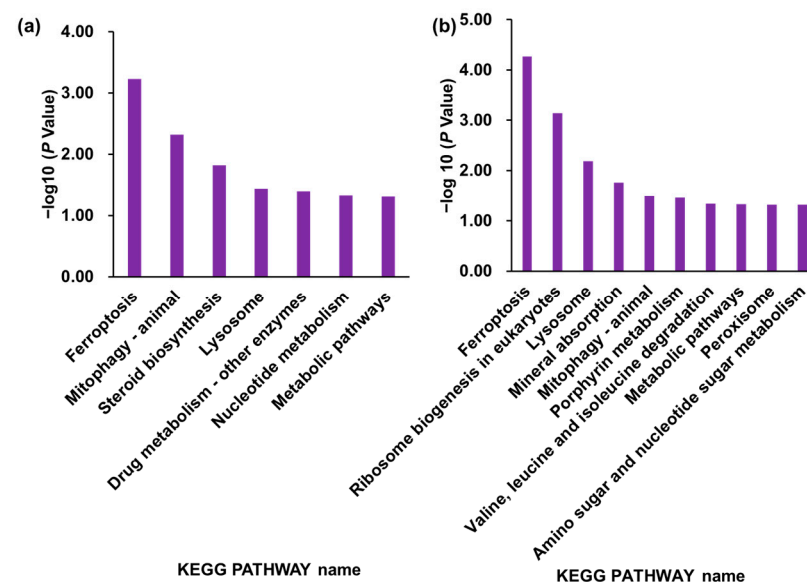


Figure 5. Enrichment analysis in the KEGG pathway from the results of the label-free global proteomics analysis. (a) KO1 versus WT using 136 DEPs in KO1. (b) KO2 versus WT using 249 DEPs in KO2. Proteins with $p < 0.05$ (Fisher’s exact test) are shown in these figures. WT—Hep G2 cells; KO1—Sites A and C mutant NPC1 model cells; KO2—Sites B and D mutant NPC1 model cells.

We performed an enrichment analysis, which is used for finding significant functions and pathways [38,40,41,66]. We used data from the Gene Ontology database (GO) and the Kyoto Encyclopedia of Genes and Genomes pathway database (KEGG) [67,68]. In the GO enrichment analysis, the results suggested that the DEPs in the KO1 cells are involved in biological processes (BPs) such as autophagy, cellular components (CCs) such as autolysosomes, and molecular function (MFs) such as RNA binding. Similarly, relationships

with many functions were suggested for the KO2 cells (Figure S6, Table S4). In the KEGG pathway enrichment analysis, seven and ten pathways were selected from the KO1 and KO2 cells as significant, respectively (Figure 5). From the KEGG pathway analysis results for both the KO1 and KO2 cells, ferroptosis (ranked No. 1 in both KO1 and KO2 cells), lysosome (ranked No. 4 in KO1 cells and ranked No.3 in KO2 cells), mitophagy (ranked No. 2 in KO1 cells and ranked No. 5 in KO2 cells), and metabolic pathways (ranked No. 7 in KO1 cells and ranked No. 8 in KO2 cells) were identified as significantly changed.

The common DEPs in the KO1 and KO2 cells were not the main DEPs observed. As mentioned above, the NPC phenotype is diverse, and patients with NPC have varied symptoms [1,2]. Conversely, the DEPs identified in both KO1 and KO2 cells could be relatively ubiquitous DEPs in NPC patients, making them more important for understanding the pathogenesis of NPC and searching for therapeutic targets. The proteins identified as DEPs and pathways in both KO1 and KO2 cells are mainly described below.

Ferroptosis is a cell death pathway catalyzed by Fe^{2+} ions and lipid peroxidation [69]. Ferroptosis has been reported to be involved in various neurodegenerative diseases, including amyotrophic lateral sclerosis, Parkinson's disease, and Alzheimer's disease [70]. However, the relationship between ferroptosis and NPC remains unclear. Regarding Fe^{2+} metabolism, abnormalities in iron homeostasis in NPC mouse models have been reported [71]. In another report, the degradation of ferritin via intracellular autophagy and the progression of ferroptosis were also identified [72]. In an enrichment analysis using the KEGG, ferroptosis was identified with increased nuclear receptor coactivator 4 (NCOA4), ferritin light chain (FTL), ferritin heavy chain (FTH1), and microtubule-associated proteins 1A/1B light chain 3B (MAP1LC3B). Of the four proteins identified in both KO1 and KO2 cells, NCOA4 is the ferritin cargo receptor required for transport into the lysosome [73,74], targeting ferritin in the autophagosome via a selective autophagic process, ferritinophagy. Both light (FTL) and heavy-chain (FTH1) subunits comprise 24-subunit spherical shell protein ferritin [75]. MAP1LC3B is known as a representative human Atg8 orthologue which binds to cargo receptors on the surfaces of autophagosomes [73]. NCOA4, FTL, FTH1, and MAP1LC3B, identified in both KO1 and KO2 cells, are all specifically related to ferritinophagy [75,76], the autophagy of ferritin for iron homeostasis [76,77]. The degradation of ferritin via ferritinophagy induces Fenton reactions by releasing ferric iron ions, resulting in the progression of ferroptosis [74,78], but it remains unclear whether increases in these DEPs cause ferritinophagy and ferroptosis or not.

For BP, the term of cellular iron ion homeostasis was identified as the seventh at KO1 and the synonymous term of iron ion homeostasis was identified as the fifth at KO2, and among the DEPs, NCOA4, FTL, and FTH1 increased and ATP-binding cassette sub-family B member 6 (ABCB6) decreased. The term represents all the processes involved in maintaining the internal steady state of iron ions at the cellular level. ABCB6 is an energy-dependent porphyrin transporter that catalyzes porphyrin transport from the cytosol to the extracellular fluid and from the cytosol to mitochondria, thereby contributing to heme biosynthesis and iron homeostasis. It is involved in the regulation of heme biosynthesis and iron homeostasis [79]. It is known that ABCB6 promote cellular defense responses against various toxic insults, so significant decreases in it in the KO1 and KO2 cells could promote the production of ROS [80,81]. In addition, the term of the intracellular sequestering of iron ion was identified in the KO1 cells (also ranked and identified in the KO2 cells with $p = 0.072$), the process through which iron ions are bound or sequestered intracellularly and separated from the other components of the biological system. From the above, many DEPs and pathways related to ferroptosis were extracted, indicating a link between ferroptosis and NPC which has been rarely reported.

NPC is a type of LSD, and changes in the expression of various proteins in lysosomes have been reported as the respective substrates accumulate in lysosomes due to deficiencies in lysosome hydrolases or transporters as well as NPC1 [10–13]. Lysosomes were identified via the KEGG analysis in both KO1 and KO2 cells, with decreased lysosomal acid glucosylceramidase (GBA) and lysosomal alpha-mannosidase (MAN2B1) and increased CD63

antigen (CD63). For CCs, autolysosomes were identified at the second and thirteenth positions in the KO1 and KO2 cells, respectively, and NCOA4, FTL, FTH1, and sequestosome-1 (SQSTM1) were increased. In CCs, autolysosomes are a type of secondary lysosome in which the primary lysosome is fused to the outer membrane of an autophagosome.

Although not included in the term of the autolysosomes of the CC, VIM is a DEP associated with autolysosomes. VIM is a type of intermediate diameter filament that anchors and supports intracellular organelles in mesenchymal cells such as fibroblasts and Schwann cells [82]. VIM plays a physiological role in the positioning of autophagosomes and lysosomes and has been shown to be an important factor in the regulation of autophagy. It has been reported that the inhibition of VIM results in the accumulation of autophagosomes and the inhibition of autophagy [83,84]. In the present measurement, VIM and nestin, an intermediate diameter filament that interacts with VIM in neurons, were increased in both the KO1 and KO2 cells. In the NPC1 knockout cells, the phosphorylation of the intermediate filament VIM was decreased compared to the WT cells, and this hypophosphorylation results from reduced protein kinase C activity [85]. It has been reported that the intracellular translocation of LDL-derived cholesterol from lysosomes is a VIM-dependent process, and the activation of protein kinase C solubilizes VIM and eliminates the accumulation of cholesterol [86,87].

GBA and MAN2B1 are both lysosomal hydrogenases. Unlike Niemann–Pick disease types A and B, which are caused by a deficiency in acid sphingomyelinase, deficits in lysosomal enzymes are not direct causes of NPC. However, secondary alterations of lysosomal enzymes in NPC have been reported [88,89], which were identified as DEPs. GBA is responsible for the degradation of glucosylceramide in lysosomes [90]. A marked decrease in activity due to mutations in the *GBA* leads to Gaucher’s disease, a type of LSD like NPC which results in the accumulation of glucosylceramide and secondary cholesterol accumulation [91]. Several reports have shown that the mass of GBA is reduced in NPC [16,92,93], which is consistent with the results of the proteome variation analyses of the KO1 and KO2 cells in this study. It has been reported that in NPC, cholesterol accumulation decreases GBA, and cholesterol depletion restores GBA levels [92]. GBA2, a glucosylceramide hydrolyzing enzyme present outside the lysosome, has been reported to be particularly abundant in Purkinje cells (PCs), one of the neuronal populations most affected by NPC, in a compensatory manner due to reduced GBA. In *Npc1* $-/-$ mice, GBA2 was found to be reduced in brain-permeable low-nanomolar inhibitors with significantly improved motor coordination and prolonged lifespan despite no improvement in cholesterol or ganglioside abnormalities. It is suggested that GBA2 activity is a therapeutic target for NPC [94]. Note that although GBA2 was identified in all cell types in this study, no significant changes were observed. In addition, miglustat, an inhibitor of ceramide glucosyltransferase, the enzyme responsible for the synthesis of glucosylceramides, is the only currently approved drug for the treatment of NPC. These results suggest that GBA and GBA2 are involved in pathogenesis in relation to glucosylceramide accumulation in NPC and could even be therapeutic targets.

Lysosomal alpha-mannosidase (MAN2B1) is a lysosomal protein that hydrolyzes the alpha-linked terminal mannose of glycoproteins. Defects in MAN2B1 cause alpha-mannosidosis, which is an autosomal recessive genetic disorder and an LSD like NPC. In alpha-mannosidosis, oligosaccharides including mannose accumulate in lysosomes [95]. Symptoms include mental and cognitive impairments, hearing loss, and ataxia, with a wide range of onset dates and similar symptoms to those observed in NPC [96,97]. MAN2B1 is also known to be associated with Parkinson’s disease, which is a neurodegenerative disease like NPC and has been reported to be a promising biomarker candidate in cerebrospinal fluid from patients with Parkinson’s disease [98]. In another report, MAN2B1 was decreased in the liver of Niemann–Pick-disease-model mice, which is consistent with the results in the KO1 and KO2 cells observed in the present study [99]. Thus, MAN2B1 has been associated with LSDs and neurodegenerative diseases, and the observed decrease in MAN2B1 could have important implications in Niemann–Pick disease.

CD63, also known as lysosomal membrane-associated protein 3 (LAMP3), is found primarily in the inner membrane of late endosomes [100]. It is also abundant in extracellular vesicles, and CD63 regulates the efflux of ferritin-Fe²⁺ complexes bound to the cargo protein NCOA4 via extracellular vesicles [101]. It has been reported that CD63 expression increases in response to intracellular iron loading and decreases in response to deficiency. The expression of CD63 is regulated by iron via the IRE-IRP system, which is responsible for regulating the expression of iron metabolism-associated proteins such as ferritin. Specifically, a canonical IRE in the 5' untranslated region of CD63 messenger RNA is responsible for regulating its expression in response to increased iron [102–104]. In this proteome variation analysis, CD63, FTL, and FTH1 were all predominantly increased, suggesting iron loading in the NPC model cells. This is consistent with previous reports of iron accumulation in the brains of NPC1 knockout mice [71].

Other proteins closely related to NPC were also identified. NPC1 was identified in all replicates in the WT cells but not in all replicates in the two types of KO cells. This is consistent with the intent of creating the cells in this study and is one basis on which the proteome reflects the pathogenesis of NPC. NPC2, one of the proteins responsible for NPC, was increased in both the KO1 and KO2 cells (by 2.1- and 1.8-fold, respectively). This is consistent with the previous proteomic analysis report [105]. Lysosome-associated membrane glycoprotein 1 (LAMP1) and lysosome-associated membrane glycoprotein 2 (LAMP2) showed significant increases (by 1.4- and 1.8-fold for KO1 and 1.4- and 1.3-fold for KO2, respectively), but were not DEPs. LAMP1 and LAMP2 account for approximately 50% of lysosomal membrane proteins and contribute to autophagy and cholesterol homeostasis [106]. LAMP1 and LAMP2 share many functions and play important roles in lysosomal cholesterol homeostasis, especially in the absence of NPC1, by binding to cholesterol and facilitating cholesterol efflux out of the lysosome [107]. These lysosomal proteins are also known in relation to other lysosomal storage diseases, such as Fabry disease, and could be associated with the neurodegenerative symptoms common to these diseases [108,109].

Mitophagy is a mitochondrial-selective form of autophagy for the elimination of damaged mitochondria [110]. The relationship between mitophagy and NPC has been widely reported. In NPC1-deficient cells, the activation of mTORC1 signaling and the associated autophagy are suppressed [111–113]. In other reports, the accumulation of cholesterol in lysosomes is observed in NPC which leads to lysosomal enlargement and the dysfunction of autophagosomes and mitochondria [114–116]. Abnormal mitochondrial clearance and a lack of mitophagy have been shown in NPC knockdown cells [117]. It was also reported that in NPC1 knockout cells, the inhibition of mTORC1 signaling resolved proteolytic defects in lysosomes and a lack of mitophagy without restoring cholesterol accumulation [118]. In the enrichment analysis, mitophagy was identified in the KEGG pathway in the KO1 and KO2 cells, with increased calcium-binding and coiled-coil domain-containing protein 2 (CALCOCO2), gamma-aminobutyric acid receptor-associated protein-like 2 (GABARAPL2), and MAP1LC3B and decreased SQSTM1. In BPs, macromitophagy was also identified at the eighth and twenty-eighth terms in the KO1 and KO2 cells, respectively, with increased MAP1LC3B and decreased SQSTM1 and GBA. Macromitophagy is defined as a selective autophagy process in which mitochondria are degraded by macroautophagy in a BP. CALCOCO2 is an autophagy adaptor, specifically known as a loading receptor for xenophagy [119]. On the other hand, it has been reported to mediate autophagosome maturation by binding to LC3B, GABARAPL2, and Myosin-VI (MYO6) in non-infected cells, suggesting that CALCOCO2 is not only involved in targeting bacterial autophagosomes, including all non-xenophagy autophagy [120]. GABARAPL2 is a member of the Atg8 orthologue as well as MAP1LC3B and is also used in mitophagy [121,122]. It has also been reported to be involved in autophagosome maturation in mitophagy in concert with CALCOCO2 and others, as mentioned above. SQSTM1 is an autophagy receptor like CALCOCO2 and others which is involved in mitophagy by recognizing ubiquitinated mitochondria together with CALCOCO2 [123,124]. Mitochondrial dysfunction based on the loss of mitophagy has been reported in knockin mice with allelic mutations of GBA [125]. De-

creased GBA could be one of the causes of the impaired degradation of NPC in lysosomes and, as mentioned above, the inhibition of mTORC1 could restore function and mitophagy. Although the relationship between the increase or decrease in DEPs and the widely reported lack of mitophagy in NPC is not clear, the fact that a mitophagy-related term was extracted at a high rank on the list in this study supports the association between NPC and mitophagy. In addition, we also reported a decrease in steroid hormone metabolism related to mitochondrial dysfunction [126] in which the steroid biosynthesis pathway was significantly altered in the KO1 cells (Figures 5a and S6).

This study was analyzed using NPC-model hepatocellular carcinoma cells, and the liver plays a pivotal role in metabolic pathways. Therefore, it is possible that there are proteins in the metabolic pathway that are closely associated with hepatosplenomegaly and other liver lesions. On the other hand, this enrichment analysis did not show any term associated with liver damage in either the GO or KEGG. In addition, many studies have been published regarding metabolic alterations, and we focused on lipid metabolism and reported its use as a diagnostic biomarker [4–7]. Amino acid alterations were reported by other groups [127,128].

There are a few proteome analyses using NPC-model cells or animals. In the two reports that analyzed the proteome using hepatocytes from NPC1 knockout mice, annexin A1, catechol-O methyltransferase (COMT), and lysosomal proteins such as cathepsin B (CTSB), cathepsin D (CTSD), and ubiquitin-like-conjugating enzyme ATG3 (ATG3) were identified as DEPs, but they were not DEPs in this analysis, although each protein was identified [129,130]. On the other hand, several common terms were identified for the GO in two reports and this analysis, including autophagy, iron homeostasis, and the heme synthesis process. In neuroblastoma cells reacted with U18666A, a process which causes symptoms similar to NPC, a number of common GO terms were identified from the top to the bottom, including the sterol biosynthesis process, cholesterol biosynthesis process, and lipid metabolic process [131]. In a proteome analysis of the cerebella of NPC1 knockout mice, lysosomal proteins such as beta-hexosaminidase subunit alpha (HEXA), beta-hexosaminidase subunit beta (HEXB), lysosomal acid lipase/cholesteryl ester hydrolase (LIPA), MAN2B1, sialidase-1 (NEU1), prosaposin (PSAP), and tripeptidyl-peptidase 1 (TPP1) were all identified as DEPs, but in the present study, none of them were identified as DEPs which showed only a slight increase or decrease except for MAN2B1. Since these measurements were performed via the LF method and not via quantification, the reproducibility between measurements for each protein is limited. Although the directions of the increase/decrease were in good agreement, the proteins detected as DEPs in these assays only suggest that they could be involved in NPC. On the other hand, a pathway analysis showed that many of the pathways were highly consistent regardless of the region being analyzed, such as the liver or brain. In the pathway analysis, rankings are determined based on variations in the results of multiple proteins, so it is possible that the LF analysis also showed results with a certain degree of reliability. In the future, therapeutic targeting should be performed based on these results.

2.4. The Accumulation of Lipid Peroxide Was Observed in Two Types of NPC Model Cells

The LF proteome variation analysis and subsequent enrichment analysis suggested a relationship between ferroptosis and NPC model cells. However, it is not clear whether ferroptosis progresses in the NPC model cells. Therefore, we measured the fluorescence induced by lipid peroxide, which characteristically accumulates with the progression of ferroptosis [77,132]. We used *tert*-butyl hydroperoxide (TBHP, 500 μ M) which induces lipid peroxidation and ferroptosis, as a positive control [133], and Liperfluo, which is widely used in the study of ferroptosis due to its lipid peroxide-specific fluorescence emission [134,135] (Figure S7). The results showed that the fluorescence intensities of both the KO1 and KO2 cells were significantly increased compared to the WT cells. Lipid peroxide accumulation was observed in the two types of NPC model cells, suggesting that ferroptosis could be underway in NPC.

On the basis of iron accumulation in NPC knockout mice, meanwhile, it has been reported that treatment with deferiprone, an iron chelator, did not extend lifespan or restore symptoms [136]. This was contrary to the results of iron chelation therapy in AD and PD, neurodegenerative diseases in which the same iron accumulation was observed, leading to neurological improvement [137,138]. However, NPC differs from these diseases in that it often develops in childhood [89]. Iron is essential for brain development, and balanced iron levels are needed, especially during growth [139]. In mice, excessive iron removal at an age of 3 months, equivalent to a human age of about 13.4 years, could lead to iron depletion during growth and a lack of therapeutic efficacy in mice. Thus, regulated iron removal or the inhibition of ferroptosis itself could be effective therapeutic targets in NPC.

There are several limitations to this study. First, further experimental validation is needed to verify the involvement of the DEPs identified in this study with molecular processes and pathways in NPC model cells. In particular, further validation is needed to demonstrate the involvement of ferroptosis, not only by showing an increase in intracellular lipid peroxides but also by showing intracellular Fe^{2+} , the accumulation of ROS, and so on [134,140]. Second, since we used an in vitro model of NPC, future studies are needed to verify the roles of DEPs and the pathways analyzed from them in the pathogenesis of NPC and their potential as therapeutic targets.

3. Materials and Methods

3.1. Chemicals and Reagents

Ultrapure water was prepared using a Puric- α apparatus (Organo Corporation, Tokyo, Japan). Acetonitrile was purchased from Kanto Kagaku (Tokyo, Japan); formic acid, methanol, and chloroform were purchased from FUJIFILM Wako Pure Chemical Co. Ltd. (Osaka, Japan); and the nano-HPLC ODS capillary column (75 $\mu\text{m} \times 12.5 \text{ cm}$, 3 μm) was acquired from Nikkyo Technos (Tokyo, Japan). The iodoacetamide (IAA), sodium dodecyl sulfate (SDS), tris(2-carboxyethyl) phosphine (TCEP), triethylammonium bicarbonate (TEAB), trypsin, Dulbecco's modified Eagle's medium (DMEM), and non-essential amino acid (NEAA) mixture reagents were obtained from Nacalai Tesque, Inc. (Kyoto, Japan). The Acclaim PepMap 100 trapping column (75 $\mu\text{m} \times 2 \text{ cm}$, 3 μm), M-PER™ Mammalian Protein Extraction Reagent, Pierce™ 660 nm Protein Assay Kit, Pierce™ Detergent Removal Spin Columns, and Pierce™ Peptide Desalting Spin Columns were purchased from Thermo Fisher Scientific (Waltham, MA, USA). TBHP was purchased from Tokyo Chemical Industry Co., Ltd. (Tokyo, Japan), and Liperfluo was purchased from DOJINDO LABORATORIES (Kumamoto, Japan).

3.2. LC/MS/MS Equipment, General Conditions, Data Acquisition, and Data Analysis

An EASY-nLC (Thermo Fisher Scientific) was connected to a quadrupole ion trap and an Orbitrap Fusion Tribrid tandem mass spectrometer equipped with an electrospray ionization probe (Thermo Fisher Scientific). The electrospray voltage and ion transfer tube temperature were set to 2000 V and 275 °C, respectively. The MS scan range, resolution, maximum injection time, and RF lens were set at m/z 375–1600, 60,000 Da, 50 ms, and 60%, respectively. Data acquisition was performed in the data-dependent analysis (DDA) mode under positive ion detection. High-collision dissociation (HCD) was used as the activation type. For the MS/MS analysis, the dynamic exclusion duration, intensity threshold, isolation window, HCD collision energy, and maximum injection time were set at 20 ms, 5×10^3 cps, 1.6 Da, 30%, and 35 ms, respectively.

Mixtures of formic acid/water (0.1:100, v/v) and formic acid/water/acetonitrile (0.1:20:80, $v/v/v$) were used as mobile phases A and B, respectively. The flow rate was set at 300 nL/min. A Nano HPLC capillary ODS column (75 μm i.d. \times 12.5 cm, 3 μm ; Nikkyo Technos) and Acclaim PepMap 100 (75 μm i.d. \times 2 cm, 3 μm ; Thermo Fisher Scientific) were used as the analytical and trapping columns, respectively. The equilibration of the analytical and trapping columns was performed using flows of 5 and 7 μL of the initial mobile phase, respectively.

Data acquisition was performed using Xcalibur (version 4.3, Thermo Fisher Scientific, accessed on 10 June 2022) and Proteome Discoverer (version 2.5.0.400, Thermo Fisher Scientific, accessed on 10 June 2022) for data integration. Proteins were identified using the UniProt database (Version 2022_05, accessed on 10 June 2022). The maximum number of cleavage misses was set to 2. The carbamidomethylation of cysteine was considered a fixed modification, and the oxidation of methionine and the N-terminal acetylation of the protein were considered variable modifications. Proteins were identified with a false discovery rate (FDR) of less than 1%. Measurements for each sample were standardized via summed intensity. When comparing two cell types, proteins with a missing value in more than 20% of replicates from one cell type were excluded from the analysis. A PCA was performed using Metaboanalyst (Version 5.0, set to default, accessed on 11 October 2023). PPI networks were constructed using STRING (version 11.0, with a minimum required interaction score set to medium confidence (0.4), accessed on 10 October 2023) [141]. The GO and KEGG enrichment analyses were carried out using the DAVID database (version 2022_04, set to default, accessed on 14 February 2023) [142].

3.3. The Establishment of NPC Cell Models

NPC cell models were developed using the CRISPR/Cas9 method [53–55] summarized in Figure S3. Hep G2 cells (WT) were used in this study. The NPC1 gene located on chromosome 18 (18q11.2.) contains 80,715 bases and 25 exons (Figure S3a) [57]. In this study, two types of knockout model cells were established by targeting multiple sites of the NPC1 gene (Figure S3). The NPC KO model cell KO1 was developed using two sgRNAs targeting 238–257 bp's on exon 1 (Site A) and 1357–1376 bp's on exon 8 (Site C) (Figure S3b). The other model (KO2) was developed using two sgRNAs targeting 279–301 bp's on exon 1 (Site B) and 3589–3611 bp's on exon 22 (Site D) (Figure S3c). Using GGGenome (<https://gggenome.dbcls.jp/ja/>, accessed on 27 March 2019) and UCSC Genome Browser (<https://genome.ucsc.edu/>, accessed on 27 March 2019) software, we selected each CRISPR targeting site of the NPC1 gene which showed no homology with other genes. HepG2 WT cells were seeded in 10 cm dishes on day 0 and transfected with px330-based CRISPR/Cas9 vectors (Figure S1) twice on days 2 and 3. On day 5, cell cloning was performed. From the cells targeting Site A and Site C, 22 clones were obtained, and KO1 was selected as a typical clone. From the cells targeting Site B and Site D, 18 clones were obtained, and KO2 was selected as a typical clone. From genomic sequencing, KO1 has a deletion of g at nt1373, an insertion of g after nt1373, and a large deletion between nt241 and nt1373, and KO2 has a tc deletion at nt283 and nt284, an insertion of g after nt283, and a large deletion between nt284 and nt3593. For the confirmation of NPC1 KO, an immunoblot analysis using an NPC1 antibody (#ab55706, Abcam, Cambridge, UK) [118,143], filipin staining [13,56], and cholesterol quantification with cholesterol E-test Wako [126] were performed (Figures S1 and S2 and Figure 1).

3.4. Cell Culture and Cellular Protein Extraction

The WT, KO1, and KO2 cells developed were cultured in DMEM containing 10% FBS, penicillin–streptomycin, and NEAA. The 2.0×10^6 cells were seeded in a 100 mm Petri dish and grown in the medium. After confluent cultures, the cells were washed twice with 3 mL of PBS and subsequently removed from the Petri dish using a scraper in 10 mL of PBS. The suspended cells were counted using a cell counter, and equal numbers of cells were frozen.

The frozen cells were mixed with 1 mL of M-PER™ Mammalian Protein Extraction Reagent. The mixture was shaken for 10 min and centrifuged at $14,000 \times g$ at 4 °C for 15 min. The supernatant was transferred to another tube, and the protein concentrations were quantified using the Pierce™ 660 nm Protein Assay Kit.

A sample of the proteins (100 µg) was transferred into a separate tube and adjusted to 100 µL with a mixture of 0.1% SDS and a 100 mM TEAB aqueous solution. In succession, 5.3 µL of a mixture of 20 mM TCEP in 0.1% SDS and 100 mM TEAB was added, and the mixed solution was heated at 95 °C for 10 min. Subsequently, 1.7 µL of a mixture of

500 mM IAA in 0.1% SDS and 100 mM TEAB was added, and the solution was maintained at 25 °C for 60 min in the dark.

To this alkylated protein fraction, 428 μ L of methanol, 107 μ L of chloroform, and 321 μ L of water were added, and the solution was mixed and centrifuged at $15,000 \times g$ at 25 °C for 1 min. The supernatant was removed, and 428 μ L of methanol was added to the remaining solution. The mixture was again centrifuged at $15,000 \times g$ at 25 °C for 1 min, and the supernatant was removed. The remaining material was dried at 25 °C using a CC-105 centrifugal concentrator (TOMY, Tokyo, Japan). The dried pellet was dissolved in 100 μ L of 0.1% SDS and 100 mM TEAB. To the solution, 4 μ L of 0.5 μ g/ μ L trypsin aqueous solution was added, and the mixture was incubated at 300 rpm at 37 °C overnight. The mixture was then sequentially placed onto a Pierce™ Detergent Removal Spin Column and Pierce™ Peptide Desalting Spin Column, and the eluted solution was dried using a CC-105 centrifugal concentrator. The pellet was dissolved in 200 μ L of a mixture of 0.1% formic acid and 2% acetonitrile in water, and the solution was used as the sample (protein amount: approximately 0.5 μ g/ μ L).

3.5. nLC Condition for Label-Free Global Proteomics

The gradient program was as follows: 0–5% B over 1 min, 5–40% B over 60 min, 40–95% B over 2 min, and 95% B over 17 min (cycle time: 80 min). The injection protein volume and amount were 2 μ L and 1 μ g, respectively. The injected sample solution was diluted with mobile phase A up to 5 μ L and applied to the trapping column. Five cell dishes were prepared for each cell line and analyzed.

3.6. Cell Fluorescence Intensity Measurement

WT, KO1, and KO2 cells (40,000 cells per well) were seeded in 96-well plates, with only DMEM medium (with serum) as a background, the WT cells as a control and positive control, and the KO1 and KO2 cells as comparisons, respectively. After overnight incubation in a tissue culture incubator at 37 °C, the cells were washed with serum-free DMEM medium, 70 μ L of 10 μ M Liperfluor was added, and the cells incubated for 30 min. After washing the cells twice with Hanks' Balanced Salt Solution (HBSS), HBSS was added for background and samples, and 500 μ M TBHP was added for the positive control and incubated for 1 h. After washing the samples with HBSS twice, they were measured using an Infinite® M200 PRO (Tecan, Männedorf, Switzerland) at an excitation wavelength of 488 nm and an emission wavelength of 535 nm. The mode was set to bottom, the gain was set to optimal, and the number of flashes was set to 10. An analysis was performed by eliminating background data due to the culture medium and excluding samples with bubbles or samples with fluorescence intensities that were more negative than the background. Standard deviations were applied to error bars, and *p* values were derived using the two-tailed, unpaired Welch's *t*-test.

4. Conclusions

Here, we aimed to elucidate the pathophysiological aspects of proteomic expression. We developed NPC1 model cells using the CRISPR/Cas9 method, and global proteomic approaches were used. In result, many differentially expressed proteins were identified using the label-free method, and the two cell models exhibited different alterations; however, commonly changing proteins were also observed. To identify the differential pathways in the pathology of NPC, we performed a bioinformatics analysis. The identification of NCOA4, FTH1, FTL, and various autophagy-related proteins as DEPs and the enrichment of ferroptosis in the pathway analysis could suggest a relation between NPC and ferroptosis which has rarely been reported. Associations between neurodegenerative diseases and ferroptosis have been reported in many diseases, and our results also suggest an association with NPC, which presents with clinical neurodegenerative symptoms. In addition, other LSD-causing genes, such as the lysosomal enzymes GBA and MAN2B1 and the lysosomal membrane protein CD63, were identified as DEPs, consistent with previous reports and

supporting the association with other LSDs and reports of abnormal iron metabolism. These pathways and proteins could serve as novel therapeutic targets, and therapeutic research based on these results is expected in the future.

Supplementary Materials: The following supporting information can be downloaded at: <https://www.mdpi.com/article/10.3390/ijms242115642/s1>.

Author Contributions: Conceptualization, M.M. and N.M. (Nariyasu Mano); methodology, E.H., N.M. (Naomi Matsukawa) and M.F.; software, K.M., E.H., N.M. (Naomi Matsukawa) and M.W.; validation, K.M., E.H., N.M. (Naomi Matsukawa) and M.M.; formal analysis, K.M., E.H., N.M. (Naomi Matsukawa) and M.M.; investigation, K.M., E.H., N.M. (Naomi Matsukawa), Y.S. (Yoshitaka Shirasago), M.W., T.S., Y.S. (Yu Sato), M.K. (Masaki Kumondai) and M.F.; resources, E.H., N.M. (Naomi Matsukawa), Y.S. (Yoshitaka Shirasago), T.S., Y.S. (Yu Sato), M.K. (Masaki Kumondai), S.K., M.F., M.M. and N.M. (Nariyasu Mano); data curation, K.M., E.H., N.M. (Naomi Matsukawa), M.W. and M.M.; writing—original draft preparation, K.M. and M.M.; writing—review and editing, K.M., E.H., M.K. (Masafumi Kikuchi), S.K., M.F., M.M. and N.M. (Nariyasu Mano); visualization, K.M., E.H., N.M. (Naomi Matsukawa) and M.M.; supervision, M.M. and N.M. (Nariyasu Mano); project administration, M.M., funding acquisition, M.M. and M.F. All authors have read and agreed to the published version of the manuscript.

Funding: This study was supported in part by JSPS KAKENHI 21K07814 (Masamitsu Maekawa), 19K07075 (Masayoshi Fukasawa), the Kawano Masanori Memorial Public Interest Incorporated Foundation for Promotion of Pediatrics (Masamitsu Maekawa), and the Japanese Society of Inherited Metabolic Disease/Sanofi LSD Research Grant (Masamitsu Maekawa).

Institutional Review Board Statement: Not applicable.

Informed Consent Statement: Not applicable.

Data Availability Statement: Data is contained within the article or supplementary material.

Acknowledgments: This study was supported in part by JSPS KAKENHI 21K07814 and 19K07075 and the Kawano Masanori Memorial Public Interest Incorporated Foundation for Promotion of Pediatrics, and the Japanese Society of Inherited Metabolic Disease/Sanofi LSD Research Grant. This research was supported by the Research Support Project for Life Science and Drug Discovery (Basis for Supporting Innovative Drug Discovery and Life Science Research (BINDS)) from AMED under grant number JP22ama121019.

Conflicts of Interest: The authors declare no conflict of interest.

References

1. Vanier, M.T. Niemann-Pick Disease Type C. *Orphanet J. Rare Dis.* **2010**, *5*, 16. [[CrossRef](#)]
2. Patterson, M.C.; Hendriksz, C.J.; Walterfang, M.; Sedel, F.; Vanier, M.T.; Wijburg, F. Recommendations for the Diagnosis and Management of Niemann-Pick Disease Type C: An Update. *Mol. Genet. Metab.* **2012**, *106*, 330–344. [[CrossRef](#)]
3. Walkley, S.U.; Suzuki, K. Consequences of NPC1 and NPC2 Loss of Function in Mammalian Neurons. *Biochim. Biophys. Acta* **2004**, *1685*, 48–62. [[CrossRef](#)]
4. Maekawa, M.; Mano, N. Identification and Evaluation of Biomarkers for Niemann-Pick Disease Type C Based on Chemical Analysis Techniques. *Chromatography* **2020**, *41*, 19–29. [[CrossRef](#)]
5. Maekawa, M.; Iwahori, A.; Mano, N. Biomarker Analysis of Niemann-Pick Disease Type C Using Chromatography and Mass Spectrometry. *J. Pharm. Biomed. Anal.* **2020**, *191*, 113622. [[CrossRef](#)] [[PubMed](#)]
6. Maekawa, M.; Mano, N. Searching, Structural Determination, and Diagnostic Performance Evaluation of Biomarker Molecules for Niemann-Pick Disease Type C Using Liquid Chromatography/Tandem Mass Spectrometry. *Mass Spectrom.* **2022**, *11*, A0111. [[CrossRef](#)]
7. Maekawa, M.; Mano, N. Cutting-Edge LC-MS/MS Applications in Clinical Mass Spectrometry: Focusing on Analysis of Drugs and Metabolites. *Biomed. Chromatogr.* **2022**, *36*, e5347. [[CrossRef](#)]
8. Jiang, X.; Sidhu, R.; Orsini, J.J.; Farhat, N.Y.; Porter, F.D.; Berry-Kravis, E.; Schaffer, J.E.; Ory, D.S. Diagnosis of Niemann-Pick C1 by Measurement of Bile Acid Biomarkers in Archived Newborn Dried Blood Spots. *Mol. Genet. Metab.* **2019**, *126*, 183–187. [[CrossRef](#)]
9. Sidhu, R.; Kell, P.; Dietzen, D.J.; Farhat, N.Y.; Do, A.N.D.; Porter, F.D.; Berry-Kravis, E.; Reunert, J.; Marquardt, T.; Giugliani, R.; et al. Application of a Glycinated Bile Acid Biomarker for Diagnosis and Assessment of Response to Treatment in Niemann-Pick Disease Type C1. *Mol. Genet. Metab.* **2020**, *131*, 405–417. [[CrossRef](#)]
10. Geberhiwot, T.; Moro, A.; Dardis, A.; Ramaswami, U.; Sirrs, S.; Marfa, M.P.; Vanier, M.T.; Walterfang, M.; Bolton, S.; Dawson, C.; et al. Consensus Clinical Management Guidelines for Niemann-Pick Disease Type C. *Orphanet J. Rare Dis.* **2018**, *13*, 50. [[CrossRef](#)]

11. Kwon, H.J.; Abi-Mosleh, L.; Wang, M.L.; Deisenhofer, J.; Goldstein, J.L.; Brown, M.S.; Infante, R.E. Structure of N-Terminal Domain of NPC1 Reveals Distinct Subdomains for Binding and Transfer of Cholesterol. *Cell* **2009**, *137*, 1213–1224. [[CrossRef](#)]
12. Pentchev, P.G.; Comly, M.E.; Kruth, H.S.; Vanier, M.T.; Wenger, D.A.; Patel, S.; Brady, R.O. A Defect in Cholesterol Esterification in Niemann-Pick Disease (Type C) Patients. *Proc. Natl. Acad. Sci. USA* **1985**, *82*, 8247–8251. [[CrossRef](#)] [[PubMed](#)]
13. Pentchev, P.G.; Boothe, A.D.; Kurth, H.S. A Genetic Storage Disorder in BALB/C Mice with a Metabolic Block in Esterification of Exogenous Cholesterol. *J. Biol. Chem.* **1984**, *259*, 5784–5791. [[CrossRef](#)] [[PubMed](#)]
14. Kuchar, L.; Sikora, J.; Gulino, M.E.; Poupetova, H.; Lugowska, A.; Malinova, V.; Jahnova, H.; Asfaw, B.; Ledvinova, J. Quantitation of Plasmatic Lysosphingomyelin and Lysosphingomyelin-509 for Differential Screening of Niemann-Pick A/B and C Diseases. *Anal. Biochem.* **2017**, *525*, 73–77. [[CrossRef](#)] [[PubMed](#)]
15. Wu, C.; Iwamoto, T.; Hossain, M.A.; Akiyama, K.; Igarashi, J.; Miyajima, T.; Eto, Y. A Combination of 7-Ketocholesterol, Lysosphingomyelin and Bile Acid-408 to Diagnose Niemann-Pick Disease Type C Using LC-MS/MS. *PLoS ONE* **2020**, *15*, e0238624. [[CrossRef](#)] [[PubMed](#)]
16. Vanier, M.T. Biochemical Studies in Niemann-Pick Disease. I. Major Sphingolipids of Liver and Spleen. *Biochim. Biophys. Acta* **1983**, *750*, 178–184. [[CrossRef](#)]
17. Svennerholm, L.; Vanier, M.T. The Distribution of Lipids in the Human Nervous System. IV. Fatty Acid Composition of Major Sphingolipids of Human Infant Brain. *Brain Res.* **1973**, *55*, 413–423. [[CrossRef](#)]
18. Patterson, M.C.; Vecchio, D.; Prady, H.; Abel, L.; Wraith, J.E. Miglustat for Treatment of Niemann-Pick C Disease: A Randomised Controlled Study. *Lancet Neurol.* **2007**, *6*, 765–772. [[CrossRef](#)]
19. Jiang, X.; Sidhu, R.; Porter, F.D.; Yanjanin, N.M.; Speak, A.O.; Te Vruchte, D.T.; Platt, F.M.; Fujiwara, H.; Scherrer, D.E.; Zhang, J.; et al. A Sensitive and Specific LC-MS/MS Method for Rapid Diagnosis of Niemann-Pick C1 Disease from Human Plasma. *J. Lipid Res.* **2011**, *52*, 1435–1445. [[CrossRef](#)]
20. Porter, F.D.; Scherrer, D.E.; Lanier, M.H.; Langmade, S.J.; Molugu, V.; Gale, S.E.; Olzeski, D.; Sidhu, R.; Dietzen, D.J.; Fu, R.; et al. Cholesterol Oxidation Products Are Sensitive and Specific Blood-Based Biomarkers for Niemann-Pick C1 Disease. *Sci. Transl. Med.* **2010**, *2*, 56ra81. [[CrossRef](#)]
21. Welford, R.W.D.; Garzotti, M.; Lourenço, C.M.; Mengel, E.; Marquardt, T.; Reunert, J.; Amraoui, Y.; Kolb, S.A.; Morand, O.; Groenen, P. Plasma Lysosphingomyelin Demonstrates Great Potential as a Diagnostic Biomarker for Niemann-Pick Disease Type C in a Retrospective Study. *PLoS ONE* **2014**, *9*, e114669. [[CrossRef](#)]
22. Sidhu, R.; Mondjinou, Y.; Qian, M.; Song, H.; Kumar, A.B.; Hong, X.; Hsu, F.F.; Dietzen, D.J.; Yanjanin, N.M.; Porter, F.D.; et al. N-Acyl-O-Phosphocholineserines: Structures of a Novel Class of Lipids That Are Biomarkers for Niemann-Pick C1 Disease. *J. Lipid Res.* **2019**, *60*, 1410–1424. [[CrossRef](#)] [[PubMed](#)]
23. Maekawa, M.; Jinnoh, I.; Matsumoto, Y.; Narita, A.; Mashima, R.; Takahashi, H.; Iwahori, A.; Saigusa, D.; Fujii, K.; Abe, A.; et al. Structural Determination of Lysosphingomyelin-509 and Discovery of Novel Class Lipids from Patients with Niemann-Pick Disease Type C. *Int. J. Mol. Sci.* **2019**, *20*, 5018. [[CrossRef](#)] [[PubMed](#)]
24. Sidhu, R.; Kell, P.; Dietzen, D.J.; Farhat, N.Y.; Do, A.N.D.; Porter, F.D.; Berry-Kravis, E.; Vite, C.H.; Reunert, J.; Marquardt, T.; et al. Application of N-Palmitoyl-O-Phosphocholineserine for Diagnosis and Assessment of Response to Treatment in Niemann-Pick Type C Disease. *Mol. Genet. Metab.* **2020**, *129*, 292. [[CrossRef](#)] [[PubMed](#)]
25. Iwahori, A.; Maekawa, M.; Narita, A.; Kato, A.; Sato, T.; Ogura, J.; Sato, Y.; Kikuchi, M.; Noguchi, A.; Higaki, K.; et al. Development of a Diagnostic Screening Strategy for Niemann-Pick Diseases Based on Simultaneous Liquid Chromatography-Tandem Mass Spectrometry Analyses of N-Palmitoyl-O-Phosphocholine-Serine and Sphingosylphosphorylcholine. *Biol. Pharm. Bull.* **2020**, *43*, 1398–1406. [[CrossRef](#)] [[PubMed](#)]
26. Jiang, X.; Sidhu, R.; Mydock-McGrane, L.; Hsu, F.F.; Covey, D.F.; Scherrer, D.E.; Earley, B.; Gale, S.E.; Farhat, N.Y.; Porter, F.D.; et al. Development of a Bile Acid-Based Newborn Screen for Niemann-Pick C Disease. *Sci. Transl. Med.* **2016**, *8*, 337ra63. [[CrossRef](#)]
27. Mazzacuva, F.; Mills, P.; Mills, K.; Camuzeaux, S.; Gissen, P.; Nicoli, E.R.; Wassif, C.; te Vruchte, D.; Porter, F.D.; Maekawa, M.; et al. Identification of Novel Bile Acids as Biomarkers for the Early Diagnosis of Niemann-Pick C Disease. *FEBS Lett.* **2016**, *590*, 1651–1662. [[CrossRef](#)]
28. Maekawa, M.; Misawa, Y.; Sotoura, A.; Yamaguchi, H.; Togawa, M.; Ohno, K.; Nittono, H.; Kakiyama, G.; Iida, T.; Hofmann, A.F.; et al. LC/ESI-MS/MS Analysis of Urinary 3 β -Sulfoxy-7 β -N-Acetylglucosaminyl-5-Cholen-24-Oic Acid and Its Amides: New Biomarkers for the Detection of Niemann-Pick Type C Disease. *Steroids* **2013**, *78*, 967–972. [[CrossRef](#)]
29. Maekawa, M.; Shimada, M.; Ohno, K.; Togawa, M.; Nittono, H.; Iida, T.; Hofmann, A.F.; Goto, J.; Yamaguchi, H.; Mano, N. Focused Metabolomics Using Liquid Chromatography/Electrospray Ionization Tandem Mass Spectrometry for Analysis of Urinary Conjugated Cholesterol Metabolites from Patients with Niemann-Pick Disease Type C and 3 β -Hydroxysteroid Dehydrogenase Deficiency. *Ann. Clin. Biochem.* **2015**, *52*, 576–587. [[CrossRef](#)]
30. Maekawa, M.; Omura, K.; Sekiguchi, S.; Iida, T.; Saigusa, D.; Yamaguchi, H.; Mano, N. Identification of Two Sulfated Cholesterol Metabolites Found in the Urine of a Patient with Niemann-Pick Disease Type C as Novel Candidate Diagnostic Markers. *Mass Spectrom.* **2016**, *5*, S0053. [[CrossRef](#)]
31. Maekawa, M.; Narita, A.; Jinnoh, I.; Iida, T.; Marquardt, T.; Mengel, E.; Eto, Y.; Clayton, P.T.; Yamaguchi, H.; Mano, N. Diagnostic Performance Evaluation of Sulfate-Conjugated Cholesterol Metabolites as Urinary Biomarkers of Niemann-Pick Disease Type C. *Clin. Chim. Acta* **2019**, *494*, 58–63. [[CrossRef](#)] [[PubMed](#)]

32. Maekawa, M.; Jinnoh, I.; Narita, A.; Iida, T.; Saigusa, D.; Iwahori, A.; Nittono, H.; Okuyama, T.; Eto, Y.; Ohno, K.; et al. Investigation of Diagnostic Performance of Five Urinary Cholesterol Metabolites for Niemann-Pick Disease Type C. *J. Lipid Res.* **2019**, *60*, 2074–2081. [[CrossRef](#)] [[PubMed](#)]
33. Maekawa, M.; Miyoshi, K.; Narita, A.; Sato, T.; Sato, Y.; Kumondai, M.; Kikuchi, M.; Higaki, K.; Okuyama, T.; Eto, Y.; et al. Development of a Highly Sensitive and Rapid Liquid Chromatography-Tandem Mass Spectrometric Method Using a Basic Mobile Phase Additive to Determine the Characteristics of the Urinary Metabolites for Niemann-Pick Disease Type C. *Biol. Pharm. Bull.* **2022**, *45*, 1259–1268. [[CrossRef](#)] [[PubMed](#)]
34. Huang, J.; Zhang, P.; Solari, F.A.; Sickmann, A.; Garcia, A.; Jurk, K.; Heemskerk, J.W.M. Molecular Proteomics and Signalling of Human Platelets in Health and Disease. *Int. J. Mol. Sci.* **2021**, *22*, 9860. [[CrossRef](#)]
35. Pisitkun, T.; Shen, R.F.; Knepper, M.A. Identification and Proteomic Profiling of Exosomes in Human Urine. *Proc. Natl. Acad. Sci. USA* **2004**, *101*, 13368–13373. [[CrossRef](#)]
36. Straussman, R.; Morikawa, T.; Shee, K.; Barzily-Rokni, M.; Qian, Z.R.; Du, J.; Davis, A.; Mongare, M.M.; Gould, J.; Frederick, D.T.; et al. Tumour Micro-Environment Elicits Innate Resistance to RAF Inhibitors through HGF Secretion. *Nature* **2012**, *487*, 500–504. [[CrossRef](#)]
37. Oda, T.; Matsumoto, K. iProteomic Analysis in Cardiovascular Research. *Surg. Today* **2016**, *46*, 285–296. [[CrossRef](#)]
38. Yao, X.Q.; Liu, Z.Y.; Chen, J.Y.; Huang, Z.C.; Liu, J.H.; Sun, B.H.; Zhu, Q.A.; Ding, R.T.; Chen, J.T. Proteomics and Bioinformatics Reveal Insights into Neuroinflammation in the Acute to Subacute Phases in Rat Models of Spinal Cord Contusion Injury. *FASEB J.* **2021**, *35*, e21735. [[CrossRef](#)]
39. Vardi, A.; Pri-Or, A.; Wigoda, N.; Grishchuk, Y.; Futerman, A.H. Proteomics Analysis of a Human Brain Sample from a Mucopolidosis Type IV Patient Reveals Pathophysiological Pathways. *Orphanet J. Rare Dis.* **2021**, *16*, 39. [[CrossRef](#)]
40. Li, S.M.; Liu, W.T.; Yang, F.; Yi, Q.J.; Zhang, S.; Jia, H.L. Phosphorylated Proteomics Analysis of Human Coronary Artery Endothelial Cells Stimulated by Kawasaki Disease Patients Serum. *BMC Cardiovasc. Disord.* **2019**, *19*, 21. [[CrossRef](#)]
41. Youssef, L.; Miranda, J.; Blasco, M.; Paules, C.; Crovetto, F.; Palomo, M.; Torramade-Moix, S.; García-Calderó, H.; Tura-Ceide, O.; Dantas, A.P.; et al. Complement and Coagulation Cascades Activation Is the Main Pathophysiological Pathway in Early-Onset Severe Preeclampsia Revealed by Maternal Proteomics. *Sci. Rep.* **2021**, *11*, 3048. [[CrossRef](#)] [[PubMed](#)]
42. Langley, S.R.; Dwyer, J.; Drozdov, I.; Yin, X.; Mayr, M. Proteomics: From Single Molecules to Biological Pathways. *Cardiovasc. Res.* **2013**, *97*, 612–622. [[CrossRef](#)] [[PubMed](#)]
43. Song, J.; Herrmann, J.M.; Becker, T. Quality Control of the Mitochondrial Proteome. *Nat. Rev. Mol. Cell Biol.* **2021**, *22*, 54–70. [[CrossRef](#)]
44. Ross, A.B.; Langer, J.D.; Jovanovic, M. Proteome Turnover in the Spotlight: Approaches, Applications, and Perspectives. *Mol. Cell. Proteom.* **2021**, *20*, 100016. [[CrossRef](#)] [[PubMed](#)]
45. Doherty, M.K.; Beynon, R.J. Protein Turnover on the Scale of the Proteome. *Expert Rev. Proteom.* **2006**, *3*, 97–110. [[CrossRef](#)]
46. Nemetlu, E.; Zhang, S.; Juranic, N.O.; Terzic, A.; Macura, S.; Dzeja, P. 18O-Assisted Dynamic Metabolomics for Individualized Diagnostics and Treatment of Human Diseases. *Croat. Med. J.* **2012**, *53*, 529–534. [[CrossRef](#)]
47. Dai, D.F.; Karunadharma, P.P.; Chiao, Y.A.; Basisty, N.; Crispin, D.; Hsieh, E.J.; Chen, T.; Gu, H.; Djukovic, D.; Raftery, D.; et al. Altered Proteome Turnover and Remodeling by Short-Term Caloric Restriction or Rapamycin Rejuvenate the Aging Heart. *Aging Cell* **2014**, *13*, 529–539. [[CrossRef](#)]
48. Ivanov, M.V.; Bubis, J.A.; Gorshkov, V.; Tarasova, I.A.; Levitsky, L.I.; Solovyeva, E.M.; Lipatova, A.V.; Kjeldsen, F.; Gorshkov, M.V. DirectMS1Quant: Ultrafast Quantitative Proteomics with MS/MS-Free Mass Spectrometry. *Anal. Chem.* **2022**, *94*, 13068–13075. [[CrossRef](#)]
49. White, N.M.A.; Masui, O.; DeSouza, L.V.; Krakovska, O.; Metias, S.; Romaschin, A.D.; John Honey, R.; Stewart, R.; Pace, K.; Lee, J.; et al. Quantitative Proteomic Analysis Reveals Potential Diagnostic Markers and Pathways Involved in Pathogenesis of Renal Cell Carcinoma. *Oncotarget* **2014**, *5*, 506–518. [[CrossRef](#)]
50. Ishihama, Y. Proteomic LC-MS Systems Using Nanoscale Liquid Chromatography with Tandem Mass Spectrometry. *J. Chromatogr. A* **2005**, *1067*, 73–83. [[CrossRef](#)]
51. Label-Free LC-MS/MS Quantitative Analysis of Aqueous Humor from Keratoconic and Normal Eyes-PubMed. Available online: <https://pubmed.ncbi.nlm.nih.gov/25999673/> (accessed on 26 September 2023).
52. Schirle, M.; Bantscheff, M.; Kuster, B. Mass Spectrometry-Based Proteomics in Preclinical Drug Discovery. *Chem. Biol.* **2012**, *19*, 72–84. [[CrossRef](#)] [[PubMed](#)]
53. Ran, F.A.; Hsu, P.D.; Wright, J.; Agarwala, V.; Scott, D.A.; Zhang, F. Genome Engineering Using the CRISPR-Cas9 System. *Nat. Protoc.* **2013**, *8*, 2281–2308. [[CrossRef](#)] [[PubMed](#)]
54. Cong, L.; Ran, F.A.; Cox, D.; Lin, S.; Barretto, R.; Habib, N.; Hsu, P.D.; Wu, X.; Jiang, W.; Marraffini, L.A.; et al. Multiplex Genome Engineering Using CRISPR/Cas Systems. *Science* **2013**, *339*, 819–823. [[CrossRef](#)]
55. Shirasago, Y.; Shimizu, Y.; Tanida, I.; Suzuki, T.; Suzuki, R.; Sugiyama, K.; Wakita, T.; Hanada, K.; Yagi, K.; Kondoh, M.; et al. Occludin-Knockout Human Hepatic Huh7.5.1-8-Derived Cells Are Completely Resistant to Hepatitis C Virus Infection. *Biol. Pharm. Bull.* **2016**, *39*, 839–848. [[CrossRef](#)] [[PubMed](#)]
56. Vanier, M.T.; Latour, P. Laboratory Diagnosis of Niemann-Pick Disease Type C: The Filipin Staining Test. *Methods Cell Biol.* **2015**, *126*, 357–375. [[CrossRef](#)] [[PubMed](#)]

57. Morris, J.A.; Zhang, D.; Coleman, K.G.; Nagle, J.; Pentchev, P.G.; Carstea, E.D. The Genomic Organization and Polymorphism Analysis of the Human Niemann-Pick C1 Gene. *Biochem. Biophys. Res. Commun.* **1999**, *261*, 493–498. [[CrossRef](#)]
58. Yamamoto, T.; Nanba, E.; Ninomiya, H.; Higaki, K.; Taniguchi, M.; Zhang, H.; Akaboshi, S.; Watanabe, Y.; Takeshima, T.; Inui, K.; et al. NPC1 Gene Mutations in Japanese Patients with Niemann-Pick Disease Type C. *Hum. Genet.* **1999**, *105*, 10–16. [[CrossRef](#)]
59. Kawazoe, T.; Yamamoto, T.; Narita, A.; Ohno, K.; Adachi, K.; Nanba, E.; Noguchi, A.; Takahashi, T.; Maekawa, M.; Eto, Y.; et al. Phenotypic Variability of Niemann-Pick Disease Type C Including a Case with Clinically Pure Schizophrenia: A Case Report. *BMC Neurol.* **2018**, *18*, 117. [[CrossRef](#)]
60. Novel Compound Heterozygous Mutation in NPC1 Gene Cause Niemann-Pick Disease Type C with Juvenile Onset-PubMed. Available online: <https://pubmed.ncbi.nlm.nih.gov/32482919/> (accessed on 26 September 2023).
61. Polese-Bonatto, M.; Bock, H.; Farias, A.C.S.; Mergener, R.; Matte, M.C.; Gil, M.S.; Nepomuceno, F.; Souza, F.T.S.; Gus, R.; Giugliani, R.; et al. Niemann-Pick Disease Type C: Mutation Spectrum and Novel Sequence Variations in the Human NPC1 Gene. *Mol. Neurobiol.* **2019**, *56*, 6426–6435. [[CrossRef](#)]
62. McKay Bounford, K.; Gissen, P. Genetic and Laboratory Diagnostic Approach in Niemann Pick Disease Type C. *J. Neurol.* **2014**, *261* (Suppl. 2), 569–575. [[CrossRef](#)]
63. Ntai, I.; Kim, K.; Fellers, R.T.; Skinner, O.S.; Smith, A.D.; Early, B.P.; Savaryn, J.P.; Leduc, R.D.; Thomas, P.M.; Kelleher, N.L. Applying Label-Free Quantitation to Top down Proteomics. *Anal. Chem.* **2014**, *86*, 4961–4968. [[CrossRef](#)] [[PubMed](#)]
64. Schork, K.; Podwojski, K.; Turewicz, M.; Stephan, C.; Eisenacher, M. Important Issues in Planning a Proteomics Experiment: Statistical Considerations of Quantitative Proteomic Data. *Methods Mol. Biol.* **2021**, *2228*, 1–20. [[CrossRef](#)] [[PubMed](#)]
65. Huang, Y.; Liu, Y.; Huang, Q.; Sun, S.; Ji, Z.; Huang, L.; Li, Z.; Huang, X.; Deng, W.; Li, T. TMT-Based Quantitative Proteomics Analysis of Synovial Fluid-Derived Exosomes in Inflammatory Arthritis. *Front. Immunol.* **2022**, *13*, 800902. [[CrossRef](#)]
66. Li, X.; Dong, Y.; Tu, K.; Wang, W. Proteomics Analysis Reveals the Interleukin-35-Dependent Regulatory Mechanisms Affecting CD8+ T-Cell Functions. *Cell. Immunol.* **2020**, *348*, 104022. [[CrossRef](#)] [[PubMed](#)]
67. Kanehisa, M.; Goto, S. KEGG: Kyoto Encyclopedia of Genes and Genomes. *Nucleic Acids Res.* **2000**, *28*, 27–30. [[CrossRef](#)]
68. Kanehisa, M.; Furumichi, M.; Tanabe, M.; Sato, Y.; Morishima, K. KEGG: New Perspectives on Genomes, Pathways, Diseases and Drugs. *Nucleic Acids Res.* **2017**, *45*, D353–D361. [[CrossRef](#)]
69. Mou, Y.; Wang, J.; Wu, J.; He, D.; Zhang, C.; Duan, C.; Li, B. Ferroptosis, a New Form of Cell Death: Opportunities and Challenges in Cancer. *J. Hematol. Oncol.* **2019**, *12*, 34. [[CrossRef](#)]
70. Moujalled, D.; Strasser, A.; Liddell, J.R. Molecular Mechanisms of Cell Death in Neurological Diseases. *Cell Death Differ.* **2021**, *28*, 2029–2044. [[CrossRef](#)]
71. Hung, Y.H.; Faux, N.G.; Killilea, D.W.; Yanjanin, N.; Firnkens, S.; Volitakis, I.; Ganio, G.; Walterfang, M.; Hastings, C.; Porter, F.D.; et al. Altered Transition Metal Homeostasis in Niemann-Pick Disease, Type C1. *Metallomics* **2014**, *6*, 542–553. [[CrossRef](#)]
72. Liang, L.; Wang, H.; Yao, J.; Wei, Q.; Lu, Y.; Wang, T.; Cao, X. NPC1 Deficiency Contributes to Autophagy-Dependent Ferritinophagy in HEI-OC1 Auditory Cells. *Front. Mol. Biosci.* **2022**, *9*, 952608. [[CrossRef](#)]
73. Mancias, J.D.; Wang, X.; Gygi, S.P.; Harper, J.W.; Kimmelman, A.C. Quantitative Proteomics Identifies NCOA4 as the Cargo Receptor Mediating Ferritinophagy. *Nature* **2014**, *509*, 105. [[CrossRef](#)]
74. Hou, W.; Xie, Y.; Song, X.; Sun, X.; Lotze, M.T.; Iii, H.J.Z.; Kang, R.; Tang, D. Autophagy Promotes Ferroptosis by Degradation of Ferritin. *Autophagy* **2016**, *12*, 1425–1428. [[CrossRef](#)] [[PubMed](#)]
75. Santana-Codina, N.; Mancias, J.D. The Role of NCOA4-Mediated Ferritinophagy in Health and Disease. *Pharmaceuticals* **2018**, *11*, 114. [[CrossRef](#)] [[PubMed](#)]
76. Sun, K.; Li, C.; Liao, S.; Yao, X.; Ouyang, Y.; Liu, Y.; Wang, Z.; Li, Z.; Yao, F. Ferritinophagy, a Form of Autophagic Ferroptosis: New Insights into Cancer Treatment. *Front. Pharmacol.* **2022**, *13*, 1043344. [[CrossRef](#)] [[PubMed](#)]
77. Xie, Y.; Hou, W.; Song, X.; Yu, Y.; Huang, J.; Sun, X.; Kang, R.; Tang, D. Ferroptosis: Process and Function. *Cell Death Differ.* **2016**, *23*, 369–379. [[CrossRef](#)] [[PubMed](#)]
78. Lamark, T.; Johansen, T. Mechanisms of Selective Autophagy. *Annu. Rev. Cell Dev. Biol.* **2021**, *37*, 143–169. [[CrossRef](#)]
79. Yuan, X.; Fleming, M.D.; Hamza, I. Heme Transport and Erythropoiesis. *Curr. Opin. Chem. Biol.* **2013**, *17*, 204. [[CrossRef](#)]
80. Song, G.; Zhang, S.; Tian, M.; Zhang, L.; Guo, R.; Zhuo, W.; Yang, M. Molecular Insights into the Human ABCB6 Transporter. *Cell Discov.* **2021**, *7*, 55. [[CrossRef](#)]
81. Boswell-Casteel, R.C.; Fukuda, Y.; Schuetz, J.D. ABCB6, an ABC Transporter Impacting Drug Response and Disease. *AAPS J.* **2017**, *20*, 8. [[CrossRef](#)]
82. Chen, K.Z.; Liu, S.X.; Li, Y.W.; He, T.; Zhao, J.; Wang, T.; Qiu, X.X.; Wu, H.F. Vimentin as a Potential Target for Diverse Nervous System Diseases. *Neural Regen. Res.* **2023**, *18*, 969. [[CrossRef](#)]
83. Biskou, O.; Casanova, V.; Hooper, K.M.; Kemp, S.; Wright, G.P.; Satsangi, J.; Barlow, P.G.; Stevens, C. The Type III Intermediate Filament Vimentin Regulates Organelle Distribution and Modulates Autophagy. *PLoS ONE* **2019**, *14*, e0209665. [[CrossRef](#)]
84. Mohanasundaram, P.; Coelho-Rato, L.S.; Modi, M.K.; Urbanska, M.; Lautenschläger, F.; Cheng, F.; Eriksson, J.E. Cytoskeletal Vimentin Regulates Cell Size and Autophagy through MTORC1 Signaling. *PLoS Biol.* **2022**, *20*, e3001737. [[CrossRef](#)]
85. Walter, M.; Chen, F.W.; Tamari, F.; Wang, R.; Ioannou, Y.A. Endosomal Lipid Accumulation in NPC1 Leads to Inhibition of PKC, Hypophosphorylation of Vimentin and Rab9 Entrapment. *Biol. Cell* **2009**, *101*, 141–153. [[CrossRef](#)] [[PubMed](#)]
86. Sarria, A.J.; Panini, S.R.; Evans, R.M. A Functional Role for Vimentin Intermediate Filaments in the Metabolism of Lipoprotein-Derived Cholesterol in Human SW-13 Cells. *J. Biol. Chem.* **1992**, *267*, 19455–19463. [[CrossRef](#)] [[PubMed](#)]

87. Tamari, F.; Chen, F.W.; Li, C.; Chaudhari, J.; Ioannou, Y.A. PKC Activation in Niemann Pick C1 Cells Restores Subcellular Cholesterol Transport. *PLoS ONE* **2013**, *8*, e74169. [[CrossRef](#)]
88. Tharkeshwar, A.K.; Trekker, J.; Vermeire, W.; Pauwels, J.; Sannerud, R.; Priestman, D.A.; Te Vrucchte, D.; Vints, K.; Baatsen, P.; Decuypere, J.P.; et al. A Novel Approach to Analyze Lysosomal Dysfunctions through Subcellular Proteomics and Lipidomics: The Case of NPC1 Deficiency. *Sci. Rep.* **2017**, *7*, 41408. [[CrossRef](#)]
89. Wheeler, S.; Sillence, D.J. Niemann–Pick Type C Disease: Cellular Pathology and Pharmacotherapy. *J. Neurochem.* **2020**, *153*, 674–692. [[CrossRef](#)]
90. Brady, R.O.; Kanfer, J.N.; Shapiro, D. Metabolism of Glucocerebrosides II. Evidence of an Enzymatic Deficiency in Gaucher’s Disease. *Biochem. Biophys. Res. Commun.* **1965**, *18*, 221–225. [[CrossRef](#)]
91. Messner, M.C.; Cabot, M.C. Glucosylceramide in Humans. *Adv. Exp. Med. Biol.* **2010**, *688*, 156–164.
92. Salvio, R.; Scarpa, S.; Ciaffoni, F.; Tatti, M.; Ramoni, C.; Vanier, M.T.; Vaccaro, A.M. Glucosylceramidase Mass and Subcellular Localization Are Modulated by Cholesterol in Niemann-Pick Disease Type C. *J. Biol. Chem.* **2004**, *279*, 17674–17680. [[CrossRef](#)]
93. Pentchev, P.G.; Gal, A.E.; Booth, A.D.; Omodeo-Sale, F.; Fours, J.; Neumeyer, B.A.; Quirk, J.M.; Dawson, G.; Brady, R.O. A Lysosomal Storage Disorder in Mice Characterized by a Dual Deficiency of Sphingomyelinase and Glucocerebrosidase. *Biochim. Biophys. Acta (BBA)-Lipids Lipid Metab.* **1980**, *619*, 669–679. [[CrossRef](#)]
94. Marques, A.R.A.; Aten, J.; Ottenhoff, R.; Van Roomen, C.P.A.A.; Moro, D.H.; Claessen, N.; Veloz, M.F.V.; Zhou, K.; Lin, Z.; Mirzaian, M.; et al. Reducing GBA2 Activity Ameliorates Neuropathology in Niemann-Pick Type C Mice. *PLoS ONE* **2015**, *10*, e0135889. [[CrossRef](#)]
95. Beck, M.; Olsen, K.J.; Wraith, J.E.; Zeman, J.; Michalski, J.C.; Saftig, P.; Fogh, J.; Malm, D. Natural History of Alpha Mannosidosis a Longitudinal Study. *Orphanet J. Rare Dis.* **2013**, *8*, 1–13. [[CrossRef](#)] [[PubMed](#)]
96. Hennermann, J.B.; Raebel, E.M.; Donà, F.; Jacquemont, M.L.; Cefalo, G.; Ballabeni, A.; Malm, D. Mortality in Patients with Alpha-Mannosidosis: A Review of Patients’ Data and the Literature. *Orphanet J. Rare Dis.* **2022**, *17*, 287. [[CrossRef](#)] [[PubMed](#)]
97. Malm, D.; Riise Stensland, H.M.F.; Edvardsen, Ø.; Nilssen, Ø. The Natural Course and Complications of Alpha-Mannosidosis—a Retrospective and Descriptive Study. *J. Inher. Metab. Dis.* **2014**, *37*, 79–82. [[CrossRef](#)]
98. Karayel, O.; Virreira Winter, S.; Padmanabhan, S.; Kuras, Y.I.; Vu, D.T.; Tuncali, I.; Merchant, K.; Wills, A.M.; Scherzer, C.R.; Mann, M. Proteome Profiling of Cerebrospinal Fluid Reveals Biomarker Candidates for Parkinson’s Disease. *Cell Rep. Med.* **2022**, *3*, 100661. [[CrossRef](#)]
99. Banno, Y.; Sasaki, N.; Miyawaki, S.; Kitagawa, T.; Nozawa, Y. Properties of Lysosomal Beta-Hexosaminidase Accumulated in Niemann-Pick Mouse Liver. *Biochem. Med. Metab. Biol.* **1986**, *36*, 322–332. [[CrossRef](#)] [[PubMed](#)]
100. Kobayashi, T.; Vischer, U.M.; Rosnoble, C.; Lebrand, C.; Lindsay, M.; Parton, R.G.; Kruithof, E.K.O.; Gruenberg, J. The Tetraspanin CD63/Lamp3 Cycles between Endocytic and Secretory Compartments in Human Endothelial Cells. *Mol. Biol. Cell* **2000**, *11*, 1829–1843. [[CrossRef](#)]
101. The Association of Ferritin and Its Cargo Receptor NCOA4 with CD63. CD63 orchestrates ferritin export. *Blood* **2021**, *138*, 1387–1389. [[CrossRef](#)]
102. Yanatori, I.; Richardson, D.R.; Dhekne, H.S.; Toyokuni, S.; Kishi, F. CD63 Is Regulated by Iron via the IRE-IRP System and Is Important for Ferritin Secretion by Extracellular Vesicles. *Blood* **2021**, *138*, 1490–1503. [[CrossRef](#)]
103. Leibold, E.A.; Laudano, A.; Yu, Y. Structural Requirements of Iron-Responsive Elements for Binding of the Protein Involved in Both Transferrin Receptor and Ferritin mRNA Post-Transcriptional Regulation. *Nucleic Acids Res.* **1990**, *18*, 1819. [[CrossRef](#)]
104. Richardson, D.R.; Ponka, P. The Molecular Mechanisms of the Metabolism and Transport of Iron in Normal and Neoplastic Cells. *Biochim. Biophys. Acta* **1997**, *1331*, 1–40. [[CrossRef](#)] [[PubMed](#)]
105. Sleat, D.E.; Wiseman, J.A.; Sohar, I.; El-Banna, M.; Zheng, H.; Moore, D.F.; Lobel, P. Proteomic Analysis of Mouse Models of Niemann-Pick C Disease Reveals Alterations in the Steady-State Levels of Lysosomal Proteins within the Brain. *Proteomics* **2012**, *12*, 3499–3509. [[CrossRef](#)] [[PubMed](#)]
106. Li, J.; Pfeffer, S.R. Lysosomal Membrane Glycoproteins Bind Cholesterol and Contribute to Lysosomal Cholesterol Export. *eLife* **2016**, *5*, e21635. [[CrossRef](#)] [[PubMed](#)]
107. Pereira, E.M.; do Monte, S.J.H.; do Nascimento, F.F.; de Castro, J.A.F.; Sousa, J.L.M.; Filho, H.C.S.A.L.C.; da Silva, R.N.; Labilloy, A.; Monte Neto, J.T.; da Silva, A.S. Lysosome-Associated Protein 1 (LAMP-1) and Lysosome-Associated Protein 2 (LAMP-2) in a Larger Family Carrier of Fabry Disease. *Gene* **2014**, *536*, 118–122. [[CrossRef](#)]
108. Jehn, U.; Bayraktar, S.; Pollmann, S.; Van Marck, V.; Weide, T.; Pavenstädt, H.; Brand, E.; Lenders, M. α -Galactosidase a Deficiency in Fabry Disease Leads to Extensive Dysregulated Cellular Signaling Pathways in Human Podocytes. *Int. J. Mol. Sci.* **2021**, *22*, 11339. [[CrossRef](#)]
109. Monticelli, M.; Hay Mele, B.; Allocca, M.; Liguori, L.; Lukas, J.; Monti, M.C.; Morretta, E.; Cubellis, M.V.; Andreotti, G. Curcumin Has Beneficial Effects on Lysosomal Alpha-Galactosidase: Potential Implications for the Cure of Fabry Disease. *Int. J. Mol. Sci.* **2023**, *24*, 1095. [[CrossRef](#)]
110. Ashrafi, G.; Schwarz, T.L. The Pathways of Mitophagy for Quality Control and Clearance of Mitochondria. *Cell Death Differ.* **2013**, *20*, 31–42. [[CrossRef](#)]
111. Düvel, K.; Yecies, J.L.; Menon, S.; Raman, P.; Lipovsky, A.I.; Souza, A.L.; Triantafellow, E.; Ma, Q.; Gorski, R.; Cleaver, S.; et al. Activation of a Metabolic Gene Regulatory Network Downstream of MTOR Complex 1. *Mol. Cell* **2010**, *39*, 171. [[CrossRef](#)]

112. Settembre, C.; Zoncu, R.; Medina, D.L.; Vetrini, F.; Erdin, S.; Erdin, S.; Huynh, T.; Ferron, M.; Karsenty, G.; Vellard, M.C.; et al. A Lysosome-to-Nucleus Signalling Mechanism Senses and Regulates the Lysosome via MTOR and TFEB. *EMBO J.* **2012**, *31*, 1095. [[CrossRef](#)]
113. Kim, J.; Kundu, M.; Viollet, B.; Guan, K.L. AMPK and MTOR Regulate Autophagy through Direct Phosphorylation of Ulk1. *Nat. Cell Biol.* **2011**, *13*, 132. [[CrossRef](#)] [[PubMed](#)]
114. Elrick, M.J.; Yu, T.; Chung, C.; Lieberman, A.P. Impaired Proteolysis Underlies Autophagic Dysfunction in Niemann-Pick Type C Disease. *Hum. Mol. Genet.* **2012**, *21*, 4876–4887. [[CrossRef](#)] [[PubMed](#)]
115. Kennedy, B.E.; Madreiter, C.T.; Vishnu, N.; Malli, R.; Graier, W.F.; Karten, B. Adaptations of Energy Metabolism Associated with Increased Levels of Mitochondrial Cholesterol in Niemann-Pick Type C1-Deficient Cells. *J. Biol. Chem.* **2014**, *289*, 16278. [[CrossRef](#)]
116. Yu, W.; Gong, J.S.; Ko, M.; Garver, W.S.; Yanagisawa, K.; Michikawa, M. Altered Cholesterol Metabolism in Niemann-Pick Type C1 Mouse Brains Affects Mitochondrial Function. *J. Biol. Chem.* **2005**, *280*, 11731–11739. [[CrossRef](#)]
117. Ordonez, M.P. Defective Mitophagy in Human Niemann-Pick Type C1 Neurons Is Due to Abnormal Autophagy Activation. *Autophagy* **2012**, *8*, 1157–1158. [[CrossRef](#)] [[PubMed](#)]
118. Davis, O.B.; Shin, H.R.; Lim, C.Y.; Wu, E.Y.; Kukurugya, M.; Maher, C.F.; Perera, R.M.; Ordonez, M.P.; Zoncu, R. NPC1-MTORC1 Signaling Couples Cholesterol Sensing to Organelle Homeostasis and Is a Targetable Pathway in Niemann-Pick Type C. *Dev. Cell* **2021**, *56*, 260–276.e7. [[CrossRef](#)] [[PubMed](#)]
119. Thurston, T.L.M.; Wandel, M.P.; Von Muhlinen, N.; Foeglein, Á.; Randow, F. Galectin-8 Targets Damaged Vesicles for Autophagy to Defend Cells against Bacterial Invasion. *Nature* **2012**, *482*, 414. [[CrossRef](#)]
120. Verlhac, P.; Viret, C.; Faure, M. Dual Function of CALCOCO2/NDP52 during Xenophagy. *Autophagy* **2015**, *11*, 965. [[CrossRef](#)]
121. Towers, C.G.; Wodetzki, D.K.; Thorburn, J.; Smith, K.R.; Caino, M.C.; Thorburn, A. Mitochondrial Derived Vesicles Compensate for Loss of LC3-Mediated Mitophagy. *Dev. Cell* **2021**, *56*, 2029. [[CrossRef](#)]
122. Weidberg, H.; Shvets, E.; Shpilka, T.; Shimron, F.; Shinder, V.; Elazar, Z. LC3 and GATE-16/GABARAP Subfamilies Are Both Essential yet Act Differently in Autophagosome Biogenesis. *EMBO J.* **2010**, *29*, 1792–1802. [[CrossRef](#)]
123. Yamada, T.; Dawson, T.M.; Yanagawa, T.; Iijima, M.; Sesaki, H. SQSTM1/P62 Promotes Mitochondrial Ubiquitination Independently of PINK1 and PRKN/Parkin in Mitophagy. *Autophagy* **2019**, *15*, 2012–2018. [[CrossRef](#)] [[PubMed](#)]
124. Wang, S.; Long, H.; Hou, L.; Feng, B.; Ma, Z.; Wu, Y.; Zeng, Y.; Cai, J.; Zhang, D.; Zhao, G. The Mitophagy Pathway and Its Implications in Human Diseases. *Signal Transduct. Target. Ther.* **2023**, *8*, 304. [[CrossRef](#)] [[PubMed](#)]
125. Li, H.; Ham, A.; Ma, T.C.; Kuo, S.H.; Kanter, E.; Kim, D.; Ko, H.S.; Quan, Y.; Sardi, S.P.; Li, A.; et al. Mitochondrial Dysfunction and Mitophagy Defect Triggered by Heterozygous GBA Mutations. *Autophagy* **2019**, *15*, 113. [[CrossRef](#)] [[PubMed](#)]
126. Abe, A.; Maekawa, M.; Sato, T.; Sato, Y.; Kumondai, M.; Takahashi, H.; Kikuchi, M.; Higaki, K.; Ogura, J.; Mano, N. Metabolic Alteration Analysis of Steroid Hormones in Niemann-Pick Disease Type C Model Cell Using Liquid Chromatography/Tandem Mass Spectrometry. *Int. J. Mol. Sci.* **2022**, *23*, 4459. [[CrossRef](#)] [[PubMed](#)]
127. Kennedy, B.E.; Hundert, A.S.; Goguen, D.; Weaver, I.C.G.; Karten, B. Presymptomatic Alterations in Amino Acid Metabolism and DNA Methylation in the Cerebellum of a Murine Model of Niemann-Pick Type C Disease. *Am. J. Pathol.* **2016**, *186*, 1582–1597. [[CrossRef](#)] [[PubMed](#)]
128. Yadid, G.; Sotnik-Barkai, I.; Tornatore, C.; Baker-Cairns, B.; Harvey-White, J.; Pentchev, P.G.; Goldin, E. Neurochemical Alterations in the Cerebellum of a Murine Model of Niemann-Pick Type C Disease. *Brain Res.* **1998**, *799*, 250–256. [[CrossRef](#)]
129. Pergande, M.R.; Cougnoux, A.; Rathnayake, R.A.C.; Porter, F.D.; Cologna, S.M. Differential Proteomics Reveals MiR-155 as a Novel Indicator of Liver and Spleen Pathology in the Symptomatic Niemann-Pick Disease, Type C1 Mouse Model. *Molecules* **2019**, *24*, 994. [[CrossRef](#)]
130. Balboa, E.; Marín, T.; Oyarzún, J.E.; Contreras, P.S.; Hardt, R.; van den Bosch, T.; Alvarez, A.R.; Rebolledo-Jaramillo, B.; Klein, A.D.; Winter, D.; et al. Proteomic Analysis of Niemann-Pick Type C Hepatocytes Reveals Potential Therapeutic Targets for Liver Damage. *Cells* **2021**, *10*, 2159. [[CrossRef](#)]
131. Cougnoux, A.; Pergande, M.R.; Serna-Perez, F.; Cologna, S.M. Investigation of 2-Hydroxypropyl- β -Cyclodextrin Treatment in a Neuronal-Like Cell Model of Niemann-Pick Type C Using Quantitative Proteomics. *J. Am. Soc. Mass Spectrom.* **2023**, *34*, 668–675. [[CrossRef](#)]
132. Tang, M.; Chen, Z.; Wu, D.; Chen, L. Ferritinophagy/Ferroptosis: Iron-Related Newcomers in Human Diseases. *J. Cell. Physiol.* **2018**, *233*, 9179–9190. [[CrossRef](#)]
133. Wenz, C.; Faust, D.; Linz, B.; Turmann, C.; Nikolova, T.; Bertin, J.; Gough, P.; Wipf, P.; Schröder, A.S.; Krautwald, S.; et al. T-BuOOH Induces Ferroptosis in Human and Murine Cell Lines. *Arch. Toxicol.* **2017**, *92*, 759–775. [[CrossRef](#)] [[PubMed](#)]
134. Stockwell, B.R.; Friedmann Angeli, J.P.; Bayir, H.; Bush, A.I.; Conrad, M.; Dixon, S.J.; Fulda, S.; Gascón, S.; Hatzios, S.K.; Kagan, V.E.; et al. Ferroptosis: A Regulated Cell Death Nexus Linking Metabolism, Redox Biology, and Disease. *Cell* **2017**, *171*, 273–285. [[CrossRef](#)] [[PubMed](#)]
135. Tsukui, T.; Chen, Z.; Fuda, H.; Furukawa, T.; Oura, K.; Sakurai, T.; Hui, S.P.; Chiba, H. Novel Fluorescence-Based Method to Characterize the Antioxidative Effects of Food Metabolites on Lipid Droplets in Cultured Hepatocytes. *J. Agric. Food Chem.* **2019**, *67*, 9934–9941. [[CrossRef](#)] [[PubMed](#)]
136. Hung, Y.H.; Lotan, A.; Yeshurun, S.; Schroeder, A.; Bush, A.I. Iron Chelation by Deferiprone Does Not Rescue the Niemann-Pick Disease Type C1 Mouse Model. *Biometals* **2020**, *33*, 87–95. [[CrossRef](#)]

137. Devos, D.; Moreau, C.; Devedjian, J.C.; Kluza, J.; Petrault, M.; Laloux, C.; Jonneaux, A.; Ryckewaert, G.; Garçon, G.; Rouaix, N.; et al. Targeting Chelatable Iron as a Therapeutic Modality in Parkinson's Disease. *Antioxid. Redox Signal.* **2014**, *21*, 195–210. [[CrossRef](#)]
138. Martin-Bastida, A.; Ward, R.J.; Newbould, R.; Piccini, P.; Sharp, D.; Kabba, C.; Patel, M.C.; Spino, M.; Connelly, J.; Tricta, F.; et al. Brain Iron Chelation by Deferiprone in a Phase 2 Randomised Double-Blinded Placebo Controlled Clinical Trial in Parkinson's Disease. *Sci. Rep.* **2017**, *7*, 1398. [[CrossRef](#)]
139. Wessling-Resnick, M. Excess Iron: Considerations Related to Development and Early Growth. *Am. J. Clin. Nutr.* **2017**, *106*, 1600S. [[CrossRef](#)]
140. Dixon, S.J.; Lemberg, K.M.; Lamprecht, M.R.; Skouta, R.; Zaitsev, E.M.; Gleason, C.E.; Patel, D.N.; Bauer, A.J.; Cantley, A.M.; Yang, W.S.; et al. Ferroptosis: An Iron-Dependent Form of Nonapoptotic Cell Death. *Cell* **2012**, *149*, 1060–1072. [[CrossRef](#)]
141. Szklarczyk, D.; Gable, A.L.; Nastou, K.C.; Lyon, D.; Kirsch, R.; Pyysalo, S.; Doncheva, N.T.; Legeay, M.; Fang, T.; Bork, P.; et al. The STRING Database in 2021: Customizable Protein–Protein Networks, and Functional Characterization of User-Uploaded Gene/Measurement Sets. *Nucleic Acids Res.* **2021**, *49*, D605–D612. [[CrossRef](#)]
142. Huang, D.W.; Sherman, B.T.; Lempicki, R.A. Systematic and Integrative Analysis of Large Gene Lists Using DAVID Bioinformatics Resources. *Nat. Protoc.* **2008**, *4*, 44–57. [[CrossRef](#)]
143. Ong, Q.R.; Lim, M.L.; Chua, C.C.; Cheung, N.S.; Wong, B.S. Impaired Insulin Signaling in an Animal Model of Niemann-Pick Type C Disease. *Biochem. Biophys. Res. Commun.* **2012**, *424*, 482–487. [[CrossRef](#)] [[PubMed](#)]

Disclaimer/Publisher's Note: The statements, opinions and data contained in all publications are solely those of the individual author(s) and contributor(s) and not of MDPI and/or the editor(s). MDPI and/or the editor(s) disclaim responsibility for any injury to people or property resulting from any ideas, methods, instructions or products referred to in the content.